

Complementarity of DM Searches in a Consistent Simplified Model: the Case of Z'

Thomas Jacques,^a Andrey Katz,^{b,c} Enrico Morgante,^c Davide Racco,^c
Mohamed Rameez,^d and Antonio Riotto^c

^aSISSA and INFN, via Bonomea 265, 34136 Trieste, Italy

^bTheory Division, CERN, CH-1211 Geneva 23, Switzerland

^cDépartement de Physique Théorique and Center for Astroparticle Physics (CAP),
Université de Genève, 24 quai Ansermet, CH-1211 Genève 4, Switzerland

^dDépartement de Physique Nucléaire et Corpusculaire,
Université de Genève, 24 quai Ansermet, CH-1211 Genève 4, Switzerland

E-mail: thomas.jacques@sissa.it, andrey.katz@cern.ch,
enrico.morgante@unige.ch, davide.racco@unige.ch,
mohamed.rameez@unige.ch, antonio.riotto@unige.ch

ABSTRACT: We analyze the constraints from direct and indirect detection on fermionic Majorana Dark Matter (DM). Because the interaction with the Standard Model (SM) particles is spin-dependent, *a priori* the constraints that one gets from neutrino telescopes, the LHC and direct detection experiments are comparable. We study the complementarity of these searches in a particular example, in which a heavy Z' mediates the interactions between the SM and the DM. We find that in most cases IceCube provides the strongest bounds on this scenario, while the LHC constraints are only meaningful for smaller dark matter masses. These light masses are less motivated by thermal relic abundance considerations. We show that the dominant annihilation channels of the light DM in the Sun are either $b\bar{b}$ or $t\bar{t}$, while the heavy DM annihilation is completely dominated by Zh channel. The latter produces a hard neutrino spectrum which has not been previously analyzed. We study the neutrino spectrum yielded by DM and recast IceCube constraints to allow proper comparison with constraints from direct detection experiments and LHC exclusions.

Contents

1	Introduction	1
2	Z'-Mediated Spin-Dependent Interactions	3
2.1	Direct constraints on Z' from LHC searches	6
2.2	DM annihilation to SM particles	7
2.3	Calculation of DM relic density	8
3	Overview of direct and indirect bounds	9
3.1	Direct Detection Experiments	9
3.2	LHC monojet constraints	11
3.3	Neutrino Telescopes – IceCube	11
3.4	Results for the Branching Ratios	14
4	Summary of results	15
5	Conclusions	19
A	Details of the annihilation rate calculation	21

1 Introduction

Although there is overwhelming evidence that Dark Matter (DM) comprises nearly a quarter of the energy budget of the Universe [1], the precise nature of the DM still remains unknown. Until now all the evidence for DM has come from gravitational interactions, while searches for other DM interactions have yielded negative results. However, nowadays there is a well-developed program of searches for DM via its presumed non-gravitational interactions. This program includes direct detection experiments, a plethora of various LHC searches, indirect searches for the annihilation of DM captured by the Earth and the Sun, as well as searches for DM annihilations in the Milky Way Galactic center and in nearby dwarf Galaxies.

One of the main motivations for thinking about DM interactions beyond the gravitational is the idea of thermal freezeout. This idea finds its natural home in the so-called WIMP-miracle scenario: a particle χ with a mass of order $\sim\text{TeV}$, charged under a weak force, yields the measured relic abundance. Direct detection experiments have mostly been aiming to discover this particular DM candidate, which also looked very attractive as part of a solution to the SM naturalness problem, in particular via supersymmetry and extra-dimensional scenarios.

The strongest bounds on the spin-independent DM-proton scattering cross-section in most cases are coming from LUX [2] that constrains this scattering at the level of $\sigma_{\chi p} \sim$

$10^{-44} \div 10^{-45} \text{ cm}^2$. These cross sections are much smaller than the natural cross sections one would expect from the WIMP miracle, and, in fact, they are more characteristic of “higgs-portal” DM [3, 4]. These direct detection results are very suggestive and put the entire idea of WIMPs under pressure.

However, there are of course several noticeable caveats in this logic, with the most important being the possibility of spin-dependent (SD) DM. If the nucleon-DM scattering rate depends on the spin of the nucleus, the *total* cross section in direct detection experiments is reduced by orders of magnitude. The strongest direct detection bounds on SD DM, coming from PICO [5], constrain $\sigma_{\chi p}^{\text{SD}} \lesssim 10^{-38} \div 10^{-39} \text{ cm}^2$, perfectly within the naive ballpark of the WIMP DM. LUX constraints on the SD DM are comparable to those of PICO [6].

Interestingly, at least naively, the direct detection bounds are not the strongest bounds one can put on the SD nucleon-DM scattering. Even stronger exclusions have been claimed both by IceCube and by collider searches at the LHC. However, these constraints are more model dependent and the comparison of these constraints to the direct detection operators is not straightforward.

The problem with comparing these results is twofold. Let us first consider the signal in neutrino telescopes. Assuming that the DM capture and annihilation rates are already in equilibrium in the Sun’s core, the total neutrino flux is only proportional to the capture rate, and independent of the DM annihilation rate [7]. However, in order to know the predicted neutrino flux, one should also know the annihilation channels. As we will discuss later, these are highly model dependent. The IceCube collaboration reports its results [8, 9] considering annihilations into WW , $\tau\tau$ (optimistic scenarios with hard neutrinos) and $b\bar{b}$ (pessimistic scenario with soft neutrinos). However, there is no guarantee that in a full UV complete picture any of these channels is dominant. In fact, if the DM is a Dirac fermion, it will most likely annihilate into a pair of SM fermions, and assuming flavor universality, these will most likely be light flavors, leaving no distinctive signature at IceCube. On the other hand, if the DM is Majorana and the fermion current preserves chirality, the light fermion channels are velocity-suppressed, giving way to other channels: WW , ZZ , hh , Zh and $t\bar{t}$. *A priori*, there is no way to know which of these channels dominates the annihilation process and sets the neutrino spectrum.

The second problem has to do with the comparison of the direct detection exclusions to the LHC searches that nominally claim the strongest bounds on SD DM interactions with nucleons. However, this claim is strongly model-dependent. The LHC searches are extremely sensitive to the ratio between the mediator couplings to the DM particles and to the SM particles. Moreover, the collider exclusions quickly weaken in the high DM mass region.

In this paper we analyze the complementarity of all these searches in one particular, but highly motivated scenario. Of course the question of complementarity is meaningless if done purely within the effective field theory (EFT) of DM. Firstly, the EFT may not include some relevant annihilation channels of DM into weak gauge bosons and the Higgs, if the particles integrated out directly interact with them. Secondly, the EFT of DM is inadequate for analyzing the results of LHC searches unless the mediator is very heavy,

otherwise the typical momentum running in the diagram is at least comparable to the mass of the mediator [10–14]. This leads to the inevitable conclusion that the question of complementarity can only be addressed in the context of full models, even if these models are simplified.

In this particular paper we will address the question of the complementarity between searches in the case that the interaction between the DM and the baryonic matter is mediated by a heavy vector boson (Z'). This is probably the easiest scenario one can consider beyond the proper WIMP (namely, the DM charged under the SM $SU(2) \times U(1)$). It can also be part of more complicated scenarios, e.g. non-minimal SUSY or strongly coupled physics at the TeV scale. We explicitly calculate the annihilation rate into the electroweak (EW) bosons and Zh and show that, if the annihilations into SM fermions are helicity suppressed, the dominant channels (depending on the DM mass) are $b\bar{b}$, $t\bar{t}$ and Zh . The latter have been neglected in previous studies, however we show that for the heavy DM it is a dominant source of hard neutrinos, which can be detected by the IceCube. Because even relatively small BRs into the gauge bosons that can potentially be important sources of the energetic neutrinos that can be detected by IceCube, we calculate the rates into the EW gauge bosons at the NLO level. We further comment on this issue in Sec. 3, while the details of the calculations are relegated to Appendix A. We show that the one-loop corrections to the WW annihilation channel are indeed important and noticeably harden the neutrino spectrum that one would naively estimate at the tree level. We also reanalyze the collider constraints, both on the direct production of Z' and on the production of DM associated with a jet.

Our paper is structured as follows. In Sec. 2 we review the basic features of SD DM, we describe in detail our setup and we review the constraints from direct searches for a Z' at colliders and from the calculation of the relic density of DM. In Sec. 3 we illustrate the constraints on our model from direct searches for DM, from the IceCube experiment, and after having discussed the branching ratios for DM pair annihilation into SM channels (which are required in order to derive bounds from IceCube) we explain how we recast the bounds from monojet searches. In Sec. 4 we illustrate our results, and in Sec. 5 we summarize our conclusions. Appendix A contains further details about the formulæ for the annihilation of DM.

2 Z' -Mediated Spin-Dependent Interactions

Spin dependent DM–baryon scattering is a fairly generic phenomenon. The non-relativistic (NR) operators that describe this scattering [15–17] have explicit dependence on the nucleus spin. These interactions can arise from different types of UV theories and studying all possible SD interactions case by case would be a tedious and unilluminating exercise. However, an $\vec{S}_\chi \cdot \vec{S}_N$ interaction, where \vec{S}_χ, \vec{S}_N are the spin of the DM particle and the nucleon respectively, is in many senses unique in the long list of NR SD operators. It is the only operator arising from an interaction mediated by a heavy particle, for which the NR limit of the DM–nucleon interaction is not also suppressed by halo velocity; that is, either powers

of \vec{q} or \vec{v} in the language of the NR EFT. These extra suppressions often render the direct detection and solar capture rates too small for most practical purposes.

In the high-energy EFT this operator descends from the axial vector - axial vector interaction [18], namely

$$\mathcal{L} = (\bar{\chi}\gamma_\mu\gamma^5\chi) (\bar{N}\gamma^\mu\gamma^5N). \quad (2.1)$$

As we have described in the introduction, this relativistic EFT description is not very useful, if we would like to compare direct detection searches for DM with the constraints from the LHC and IceCube. The UV completion for this operator is needed. There are several options for how this interaction can be completed at the renormalizable level. The simplest and most economical possibility, from the point of view of model building, is to mediate the interaction via a massive neutral vector boson, which couples to the SM axial current and to the DM axial current. This might either be a Z -boson of the SM (corresponding to a standard WIMP scenario) or a new Z' boson.

The simplest realization of this scenario would be a “classical” WIMP, namely a Majorana fermion that is charged under the SM $SU(2) \times U(1)$ (but not under the electromagnetism) and couples to the heavy weak gauge bosons at the tree level. One can view a supersymmetric electroweakino as a prototype of this kind of DM – either a doublet or a triplet of $SU(2)_L$, possibly mixed with a singlet (bino).¹ SUSY dark matter also satisfies the criteria that we have listed above: the direct detection cross-section is spin-dependent and therefore the bounds from direct detection experiments are relatively weak. Because the generic SUSY DM candidate is a Majorana fermion (rather than Dirac), annihilations into the light quarks are helicity suppressed. In the neutralino case, the annihilation into the EW gauge bosons proceeds at the leading order and in this case the WW , ZZ and $t\bar{t}$ channels dominate the annihilation branching ratios. The only relevant NLO annihilation channels for the neutralino spin-dependent DM are $\gamma\gamma$ and γZ , which have been fully analyzed in Refs. [21, 22].

Another straightforward yet less explored UV-completion is mediation of interaction (2.1) by a heavy Z' , remnant of a new gauge symmetry at the TeV scale. In particular, we assume the following renormalizable interaction between the DM, Z' mediator and the SM fermions:

$$\mathcal{L} = ig_\chi \bar{\chi}\gamma^\mu\gamma^5\chi Z'_\mu + ig_f^A \bar{\psi}\gamma^\mu\gamma^5\psi Z'_\mu + ig_f^V \bar{\psi}\gamma^\mu\psi Z'_\mu, \quad (2.2)$$

where χ is a Majorana DM particle and ψ stands for the SM fermions. Note that we have not yet specified the couplings of the Z' to the SM Higgs (if they exist at all). We expect a generic Z' to couple to both a vector and an axial current, and therefore we write down both these couplings for the SM fermions. For the DM fermions we have two choices: they might be either Dirac or Majorana fermions. If they are Dirac, it would be difficult to explain why the Z' does not couple to the vector current, opening up spin-independent scattering with baryons. On the other hand, if the DM is *Majorana*, Eq. (2.2) presents the most general couplings of the Z' to the DM and the SM fermions. Hence, we will further consider only Majorana DM.

¹For a generalization of this scenario to arbitrary representations see [19, 20].

The scenario of DM which couples to the SM via a TeV-scale Z' has been addressed in a number of references e.g. [23–42], however it is still unclear how various direct and indirect searches compare in this case. The most important caveat in this comparison has to do with the signal from neutrino telescopes, because it is very sensitive to the annihilation branching ratios of the DM into the EW bosons. The annihilation cross sections of DM into the SM fermions are helicity suppressed (except for $m_\chi \sim m_f$, with f a SM fermion, where there is no suppression into $f\bar{f}$), and therefore bosonic channels are expected to be the dominant source of neutrinos that can be detected by IceCube from DM annihilation in the Sun.

Parenthetically we note that another option for mediating the axial vector is via diagrams with new scalars in the t - and u -channels [43] (see also [44]). In this work we will put these examples aside, because of the generic problem of flavor changing neutral currents that these scalars can mediate. However it would also be interesting to see what the dominant annihilation channels are in this case.²

In this study we exclusively concentrate on the Z' mediator in the s -channel, as it appears in Eq. (2.2). Of course not every Z' with arbitrary charges would be a consistent UV-completion of the effective contact term (2.1). If the Z' is a gauge boson of a broken symmetry at multi-TeV scale, we should make sure that we are analyzing an anomaly free theory. This is a crucial demand, because without specifying the full matter content of the anomaly free theory, the annihilation rates of DM into the gauge bosons remain, strictly speaking, incalculable. Indeed, some of them could occur via loop diagrams, whose value is only guaranteed to be finite if the theory is renormalizable.

Based on the demands of renormalizability and anomaly cancellation, one can relatively easily parametrize all possible flavor-blind $U(1)'$ models. Any such model will be a linear combination of the SM hypercharge and $U(1)_{B-L}$ (see Sec. 22.4 of [45]). In extreme cases we either get a Y -sequential theory or a pure $U(1)_{B-L}$. As we will shortly see, the latter is quite a boring case for DM direct and indirect searches because it is halo-momentum suppressed.³

Because the charges of the SM fermions under the new $U(1)$ are a two-parameter family, we will conveniently parametrize the generator of the new symmetry as

$$\cos\theta t_Y + \sin\theta t_{B-L} \tag{2.3}$$

where t_Y and t_{B-L} stand for the generators of the hypercharge and $B-L$ symmetries respectively. To ensure that the fermion masses are gauge invariant, the SM fermion charges under the $U(1)'$ unambiguously determine the SM Higgs charge under the $U(1)'$. For completeness we list all the charges under the gauge symmetries, including the $U(1)'$, in Table 1.

²An obvious way to avoid dangerous FCNC would be to impose some flavor symmetries, similar to those one usually assumes in flavor-blind SUSY models.

³So-called “anomalous” $U(1)$ has also been discussed in literature, e.g. $U(1)_\psi$ [46]. Note that these models demand the introduction of spectator fermions to cancel the anomalies. One should necessarily take into account the contribution of spectators when calculating the DM annihilation branching ratios to avoid non-physical results.

	$SU(3)$	$SU(2)$	$U(1)_Y$	$U(1)_{B-L}$	$U(1)'$
$\begin{pmatrix} \nu_L^{\ell_i} \\ \ell_L^i \end{pmatrix}$	$\mathbf{1}$	$\mathbf{2}$	$-\frac{1}{2}$	-1	$-\frac{1}{2} \cos \theta - \sin \theta$
$(\ell_R^i)^C$	$\mathbf{1}$	$\mathbf{1}$	1	$+1$	$\cos \theta + \sin \theta$
$\begin{pmatrix} u_L^i \\ d_L^i \end{pmatrix}$	$\mathbf{3}$	$\mathbf{2}$	$\frac{1}{6}$	$+\frac{1}{3}$	$\frac{1}{6} \cos \theta + \frac{1}{3} \sin \theta$
$(u_R^i)^C$	$\bar{\mathbf{3}}$	$\mathbf{1}$	$-\frac{2}{3}$	$-\frac{1}{3}$	$-\frac{2}{3} \cos \theta - \frac{1}{3} \sin \theta$
$(d_R^i)^C$	$\bar{\mathbf{3}}$	$\mathbf{1}$	$\frac{1}{3}$	$-\frac{1}{3}$	$\frac{1}{3} \cos \theta - \frac{1}{3} \sin \theta$
$\Phi = \begin{pmatrix} \phi^+ \\ \phi^0 \end{pmatrix}$	$\mathbf{1}$	$\mathbf{2}$	$\frac{1}{2}$	0	$\frac{1}{2} \cos \theta$

Table 1. Charges of the SM matter content under the gauge symmetries of the SM and the gauge $U(1)'$ with the generator (2.3). i stands for the family index.

These charges have a strong impact on the DM phenomenology in this scenario. Because the SM Higgs couples to the Z' , tree level couplings between the Z' and the EW gauge bosons are induced after EW symmetry breaking. In this case Z' mixes with the Z . This allows annihilations of the DM to EW gauge bosons at the tree level.

2.1 Direct constraints on Z' from LHC searches

Here we review direct constraints on this Z' from the LHC. In addition, we will consider monojet constraints on DM production in Sec. 3.2. The easiest way to spot a Z' at a collider is via an analysis of the leptonic modes, unless they are highly suppressed. For these purposes we recast a CMS search for a narrow Z' in the leptonic channel [47], which conveniently phrases the constraints in terms of

$$R_\sigma \equiv \frac{\sigma(pp \rightarrow Z') \times BR(Z' \rightarrow l^+l^-)}{\sigma(pp \rightarrow Z) \times BR(Z \rightarrow l^+l^-)} \quad (2.4)$$

and for the reference point we take $\sigma(pp \rightarrow Z) \times BR(Z \rightarrow l^+l^-) = 1.15$ nb at $\sqrt{s} = 8$ TeV [48].

We show the results of our recast in Fig. 1 as a function of the mass $m_{Z'}$ of the Z' and the angle θ as defined in Eq. (2.3). Note that, for a given $g_{Z'}$ and θ , all couplings to the SM are fixed, therefore both production cross sections and BRs are unambiguously determined by these values. In Fig. 1 we show the exclusions both for nominal cross sections, as we get from `MadGraph5` [49], as well as for cross sections one gets by applying the flat k -factor $k = 1.3$ (similar to the suggestion in [50]). It is apparent from these lines that, in order to have a Z' with $\mathcal{O}(1)$ couplings, its mass must be $m_{Z'} \gtrsim 3$ TeV. Note that the constraints from LEP, coming from the mixing between the Z and Z' , which further affect the T -parameter, are much weaker than the direct LHC constraints.

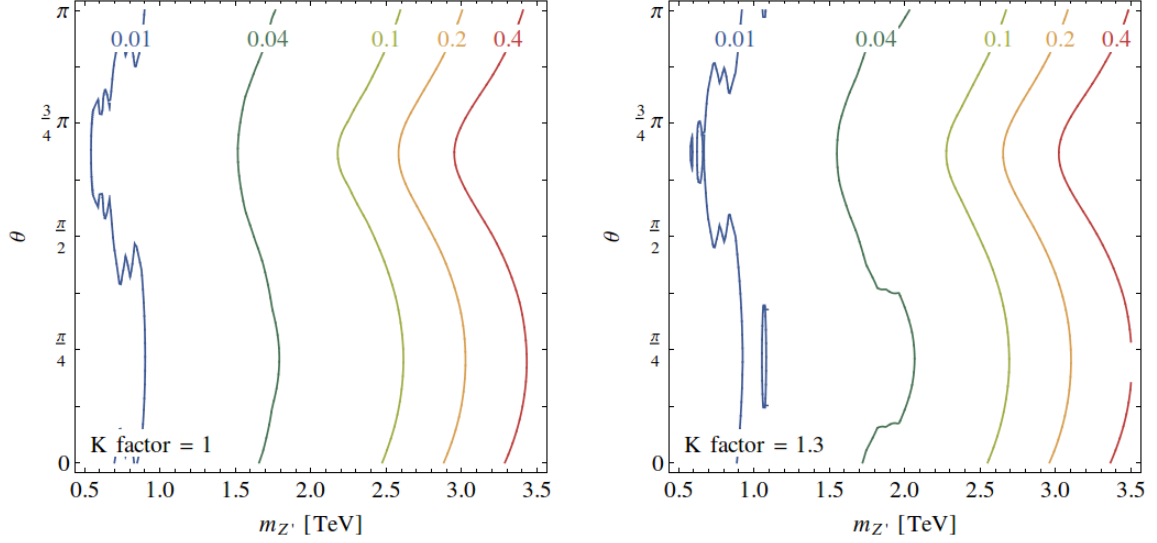


Figure 1. Maximal allowed gauge couplings $g_{Z'}$ of the hidden $U(1)'$ as a function of the angle θ (Eq. (2.3)) and of $m_{Z'}$. On the LH side we assume the nominal LO cross sections, on the RH side we apply a flat $k = 1.3$ factor.

2.2 DM annihilation to SM particles

The annihilation proceeds via Z' into the SM fermions and the EW gauge bosons. The couplings of the Z' to the EW gauge bosons, in particular to Zh and W^+W^- , arise at the *tree level* after EW symmetry breaking, when the Higgs Goldstone modes are “eaten” by the massive gauge bosons. Before EWSB one can write down the couplings of the Z' to the SM as follows:

$$\begin{aligned} \mathcal{L}_{Z'-\text{SM}} = & g_{Z'} Z'_\mu \left(\bar{e}^i (c_e^V \gamma^\mu + c_e^A \gamma^\mu \gamma_5) e^i + \bar{\nu}^i (c_\nu^V \gamma^\mu + c_\nu^A \gamma^\mu \gamma_5) \nu^i \right. \\ & \left. + \bar{u}^i (c_u^V \gamma^\mu + c_u^A \gamma^\mu \gamma_5) u^i + \bar{d}^i (c_d^V \gamma^\mu + c_d^A \gamma^\mu \gamma_5) d^i \right) + (D_\mu H)^\dagger (D^\mu H) \end{aligned} \quad (2.5)$$

with $D_\mu = D_\mu^{\text{SM}} - \frac{i}{2} \cos \theta g_{Z'} Z'_\mu$ and the vector/axial vector couplings of the Z' to the SM fermions given in Table 2. The Lagrangian describing DM is

$$\mathcal{L}_{\text{DM}} = \frac{1}{2} \bar{\chi} (i \not{\partial} - m_\chi) \chi + \frac{1}{2} g_{Z'} g_\chi Z'_\mu (\bar{\chi} \gamma^\mu \gamma_5 \chi), \quad (2.6)$$

where g_χ is the coupling of χ to the Z' . In this paper we do not consider kinetic mixing, and we neglect the effects of renormalization group equations that could mix Z and Z' via loop effects. The latter is indeed a minor effect, if the model is such that the mixing is zero at a scale close to the electroweak one. We do not specify the dynamics of the spontaneous symmetry breaking sector of $U(1)'$, and for our purposes we just assume that it provides a mass term $\frac{1}{2} m_{Z'}^2 Z'^2$.

As we expand Eq. (2.5) we find that the Z' mixes with Z , with a mixing angle ψ fully determined by the mass $m_{Z'}$ of the physical mass eigenstate, the value of the coupling $g_{Z'}$ and the angle θ . If we denote the mass of the lighter mass eigenstate by $m_Z = 91.2$ GeV,

then ψ turns out to be of order $\psi \sim g_{Z'} \cos \theta \left(\frac{m_Z}{m_{Z'}}\right)^2 \ll 1$ in the regime $m_{Z'} \gg m_Z$ that we consider in this work. For this reason, in the remainder of the paper we ignore the mixing for simplicity of notation, and denote both the interaction or mass eigenstate equivalently by Z' , and the lighter mass eigenstate identifiable with the SM vector boson by Z .

SM fermion f	g_f^V : coeff. of $g_{Z'} \bar{f} Z' f$	g_f^A : coeff. of $g_{Z'} \bar{f} Z' \gamma_5 f$
leptons	$-\frac{3}{4} \cos \theta - \sin \theta$	$-\frac{1}{4} \cos \theta$
neutrinos	$-\frac{1}{4} \cos \theta - \frac{1}{2} \sin \theta$	$\frac{1}{4} \cos \theta + \frac{1}{2} \sin \theta$
up quarks	$\frac{5}{12} \cos \theta + \frac{1}{3} \sin \theta$	$\frac{1}{4} \cos \theta$
down quarks	$-\frac{1}{12} \cos \theta + \frac{1}{3} \sin \theta$	$-\frac{1}{4} \cos \theta$

Table 2. Coefficients of the vector and axial vector bilinear currents for the SM fermions (*cf* Eq. (2.5)). With obvious meaning of the notation, the coefficients g^V and g^A are obtained from g^L, g^R of Tab. 1 via $g^L P_L + g^R P_R = \frac{g^L + g^R}{2} + \frac{-g^L + g^R}{2} \gamma_5$, so that $g^V = \frac{g^L + g^R}{2}$, $g^A = \frac{-g^L + g^R}{2}$.

Due to the Z - Z' mixing, the heavy Z' couples at tree level to Zh with a vertex

$$\frac{1}{2} \cos \theta g_{Z'} g_Z v \left(Z' Zh \right), \quad (2.7)$$

where $g_Z = \sqrt{g^2 + g'^2} = 2m_Z/v$ with $v = 246$ GeV, and with W^+W^- with a vertex equal to $\sin \psi$ times the SM vertex for ZW^+W^- ,

$$\sin \psi \cdot ig \cos \theta_W \left[\left(W_\mu^+ W_\nu^- - W_\nu^+ W_\mu^- \right) \partial^\mu Z'^\nu + W_{\mu\nu}^+ W^{-\mu} Z'^\nu - W_{\mu\nu}^- W^{+\mu} Z'^\nu \right], \quad (2.8)$$

where $W_{\mu\nu}^\pm = \partial_\mu W_\nu^\pm - \partial_\nu W_\mu^\pm$. Notice that both (2.7) and (2.8) are proportional to $\cos \theta$, thus they vanish in the pure $U(1)_{B-L}$ limit. Interaction (2.8) turns out to be velocity suppressed, thus it gives a small cross section in the low DM velocity regime of DD and IC, and both (2.7) and (2.8) are proportional to $\cos \theta$, thus vanish in the pure $U(1)_{B-L}$ limit. Because of these suppressions, loop channels are also relevant at low kinetic energy, as discussed in Sec. 3.4. In particular, the annihilation of $\chi\chi$ to Zh occurs at tree level, except for the case in which the $U(1)'$ extension is a pure $U(1)_{B-L}$ gauge symmetry. At low velocity, annihilation into W^+W^- is instead dominantly driven by diagrams with a fermionic loop (see Appendix A).

2.3 Calculation of DM relic density

Now that we have all the tree level couplings of the Z' , we are ready to calculate the thermal relic abundance of the Majorana DM. We calculate the annihilation rates and perform the thermal average using the procedure of [51]. The result for the thermally averaged self-annihilation cross section as a function of temperature T is

$$\langle \sigma v \rangle = \frac{x}{8m_\chi^5} \frac{1}{(\mathcal{K}_2(x))^2} \int_{4m_\chi^2}^{\infty} \sigma_{\text{ann}} \sqrt{s} (s - 4m_\chi^2) \mathcal{K}_1 \left(\frac{x\sqrt{s}}{m_\chi} \right) ds, \quad (2.9)$$

where $x = m_\chi/T$, and \mathcal{K}_i is the modified Bessel function of order i .

We do not approximate the thermally averaged cross section with a low DM velocity expansion, since close to the resonance $m_\chi \lesssim m_{Z'}/2$, terms of higher order can also yield important contributions to the relic density [52].

Once we fix the values of the angle θ and $m_{Z'}$, we are left with $g_{Z'}$ as the only free parameter. In Fig. 2 we show the value of $g_{Z'}$ that yields the correct relic density as measured by [1]. The areas above (below) the lines correspond to points of the parameter space where the DM is under- (over-) abundant in the thermal scenario.

For the calculation of the relic density we relied only on tree level cross sections, which we confirmed are dominant at typical freeze-out energies. Varying the value of g_χ (which for this computation was set to 1) while keeping the product $g_{Z'}\sqrt{g_\chi}$ fixed only very mildly affects the decay width $\Gamma_{Z'}$, and would have practically no effect on Fig. 2.

The lines in Fig. 2 stop at $m_\chi = m_{Z'}$: above that threshold, annihilation into $Z'Z'$ opens up, and in principle one would need to specify the details of the spontaneous symmetry breaking sector of $U(1)'$ in order to compute the relic abundance precisely. This is not required for our purpose of understanding the plausible range of values for $g_{Z'}$ that yield a relic abundance close to the observed one.

3 Overview of direct and indirect bounds

The constraints on the scenario that we have described above come from three different primary sources: direct detection, neutrino telescopes and the LHC. Since we assume a Majorana DM particle, all interactions that we get between the nuclei and the DM are either spin dependent or halo velocity suppressed, or both. We will comment on these interactions in detail in Subsec. 3.1. This particular feature renders the direct detection results much less efficient than in the case of spin-independent interactions, while other experiments, notably neutrino telescopes and the LHC, become competitive. In the following section we will carefully go through all of these different experiments and discuss the bounds that they produce.

3.1 Direct Detection Experiments

In this type of experiment, in a model with a Z' mediator the effective DM theory is always valid, because the transferred momentum never exceeds hundreds of MeV, well below the mediator scale. The effective contact terms that one gets between the DM and SM quarks are

$$\mathcal{L}_{eff} = \frac{g_q^V}{\Lambda^2} \bar{\chi} \gamma^\mu \gamma^5 \chi \bar{q} \gamma_\mu q + \frac{g_q^A}{\Lambda^2} \bar{\chi} \gamma^\mu \gamma^5 \chi \bar{q} \gamma_\mu \gamma^5 q \quad (3.1)$$

with coefficients g given in Table 2, and $1/\Lambda^2 = g_{Z'}^2 g_\chi / m_{Z'}^2$.

It is straightforward to translate these interactions to the more intuitive language of the NR effective theory. Using the dictionary of Ref. [18] and considering a nucleus N instead of the partons q we get

$$\bar{\chi} \gamma^\mu \gamma^5 \chi \bar{N} \gamma_\mu \gamma^5 N \rightarrow -4 \vec{S}_\chi \cdot \vec{S}_N = 4\mathcal{O}_4 \quad (3.2)$$

$$\bar{\chi} \gamma^\mu \gamma^5 \chi N \gamma_\mu N \rightarrow 2\vec{v} \cdot \vec{S}_\chi + 2i \vec{S}_\chi \cdot \left(\vec{S}_N \times \frac{\vec{q}}{m_N} \right) = 2\mathcal{O}_8 + 2\mathcal{O}_9. \quad (3.3)$$

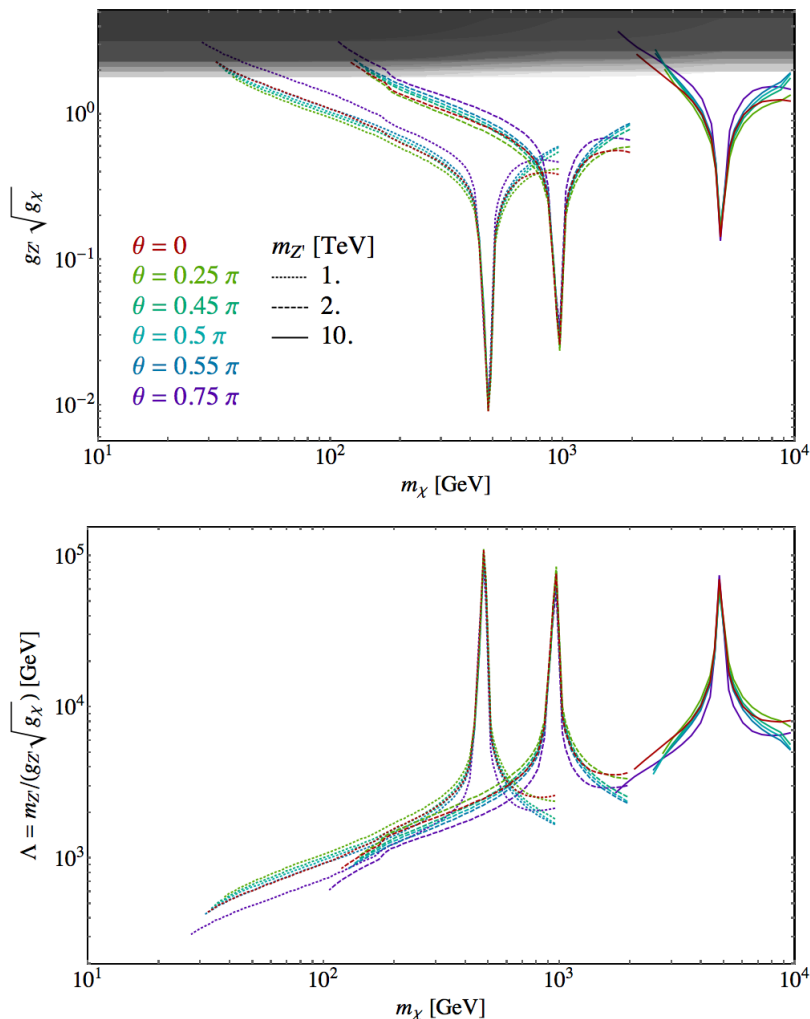


Figure 2. Top: Value of $g_{Z'}\sqrt{g_\chi}$ that yields to the correct relic density, for three masses of the Z' and different values of θ . The regions coloured with multiple shades of gray in the upper part of the plot (one for each θ , $m_{Z'}$) show the regions where $\Gamma_{Z'}$ becomes of the order of $m_{Z'}$, signalling the transition to the non-perturbative regime. Bottom: Same data as left, in the plane Λ vs. m_χ .

For a generic Z' (arbitrary θ angle in (2.3)) we get both axial current - axial current (AA) and axial current - vector current (AV) interactions with the coefficients being roughly of the same order of magnitude. However, the latter induces interactions that are halo velocity suppressed (\mathcal{O}_8) and both nuclear spin and halo velocity suppressed (\mathcal{O}_9). This usually renders the AV interactions smaller than the AA interactions for direct detection and solar capture, although we do include AV interactions when we derive our bounds. In fact, the halo-velocity suppression in \mathcal{O}_8 is sometimes comparable to the suppression due to the spin-dependence in \mathcal{O}_4 . The operator \mathcal{O}_9 , which is both spin-dependent and halo velocity dependent via the exchange momentum \vec{q} is completely negligible.

For direct detection, there is a special point in parameter space where the usual spin-dependent operator completely shuts down. This happens when our new gauge symmetry

is exactly $U(1)_{B-L}$, or, in our language, $\theta = \frac{\pi}{2}$. In this case the Z' couples only to the vector current of the SM, and therefore the NR interaction operators proceed only via \mathcal{O}_8 and subdominantly via \mathcal{O}_9 .

We derive the exclusion bounds obtained by the experiments LUX, XENON100, CDMS-Ge, COUPP, PICASSO, SuperCDMS with the help of the tables made available by [53], and the bounds by PICO from [5]. The strongest constraints among them are shown in Figs. 5 and 6, together with the constraints from IceCube and monojet searches.

3.2 LHC monojet constraints

In this section, we explore the bounds on our $U(1)'$ model coming from LHC searches for DM, analyzing events with one hard jet plus missing transverse energy (\cancel{E}_T).

Currently, the strongest exclusion limits are from the CMS analysis [54], which analyzes 19.7 fb^{-1} at a collision energy of 8 TeV.

Since we are mainly interested in the high $m_{Z'}$ regime, we can use the EFT interpretation of the exclusion bounds, as it is consistent for $m_{Z'} \gtrsim 2 \text{ TeV}$ [10, 11, 13, 14]. The effective operators describing the interaction between DM and quarks, in the high $m_{Z'}$ limit, are

$$\frac{1}{\Lambda^2} \sum_q g_q^V (\bar{\chi} \gamma^\mu \gamma_5 \chi) (\bar{q} \gamma_\mu q) \quad (3.4)$$

and

$$\frac{1}{\Lambda^2} \sum_q g_q^A (\bar{\chi} \gamma^\mu \gamma_5 \chi) (\bar{q} \gamma_\mu \gamma_5 q), \quad (3.5)$$

where $\Lambda \equiv m_{Z'}/(g_{Z'} \sqrt{g_\chi})$ and the coefficients g_q^V, g_q^A are given in Table 2.

At LHC energy scales, the occurrence of a vector or an axial vector current in the fermion bilinears in (3.4) and (3.5) does not affect the cross section for the production of DM. This is also apparent from the experimental exclusion limits reported in [54].

The CMS analysis recasts the exclusion bound as a function of the coefficient Λ of Eq. (3.5), assuming that **1**) all the g_q^A coefficients are equal to 1, and **2**) that χ is a Dirac fermion (with canonically normalized kinetic term). These two assumptions are not true for our analysis. The second assumption gives an overall factor of 2 in the cross section for the Majorana case relative to the Dirac case. We take into account both the first assumption and the convolution with the parton distribution functions (PDFs) of quarks, by means of a parton level simulation performed with MadGraph 5 [49]. We simulate the signal both with the EFT defined by CMS and with our model, and we compute for each value of θ (which determines g_q^V, g_q^A) and m_χ a rescaling factor that we use to rescale the nominal limit reported by the CMS analysis.

The final result for the bounds on Λ from monojet searches are reported in Fig. 3.

3.3 Neutrino Telescopes – IceCube

The most stringent constraint on the spin dependent WIMP-Nucleon cross section comes from IceCube, a Cherenkov neutrino detector in the deep glacial ice at the South Pole [55], through a search for neutrinos from WIMP annihilations in the Sun [56]. Let us briefly

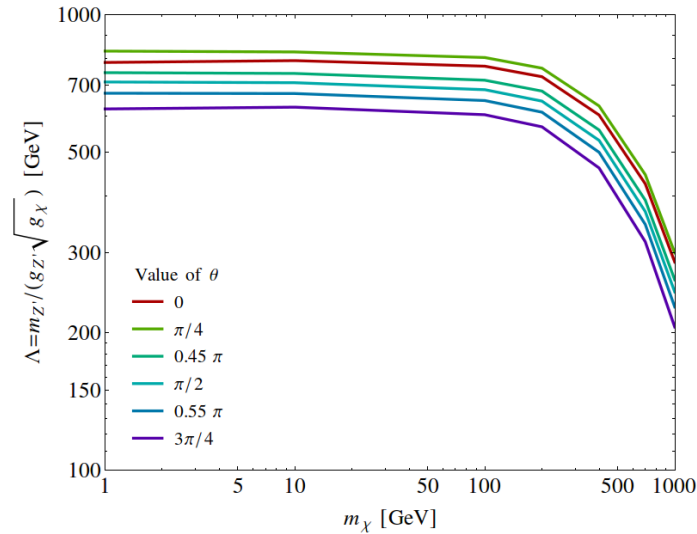


Figure 3. Bound on $\Lambda = m_{Z'}/(g_{Z'}\sqrt{g_\chi})$ as a function of m_χ , for the six values of θ shown in the legend, from the CMS monojet search [54].

review the main points of the physics related to DM annihilations in the Sun. We refer to Ref. [57] for a more detailed discussion.

DM particles in the Galactic halo can scatter with atomic nuclei inside the Sun and lose some of their energy. If the final velocity of the DM particle is low enough, it can remain gravitationally bound in the Sun. This accumulation process is counterbalanced by the evaporation process, i.e. the escape of DM particles from the Sun, and by the annihilation of DM pairs⁴ into SM particles. The evaporation process can be safely neglected, if the DM particle mass is above ~ 10 GeV. The interplay between DM capture and annihilation drives the DM number density n_{DM} towards an equilibrium. The final value of n_{DM} , and the equilibrium time by which this value is attained, depend on the capture rate Γ_{cap} and on the annihilation rate Γ_{ann} , the latter being proportional to n_{DM}^2 . When equilibrium is attained, then $\Gamma_{\text{cap}} = 2\Gamma_{\text{ann}}$, and the annihilation cross section can be directly related to the cross section of elastic scattering between DM and proton.

Neutrinos are among the final annihilation products of DM, even more so when including the electroweak (EW) corrections [58]. If the energy of the final states is above the weak scale, then electroweak interactions imply a considerable emission of EW bosons in the final state, further amplifying the neutrino flux.

We include the effects of EW corrections and of the propagation of neutrinos by means of the PPC 4 DM ID code [59, 60]. This code provides a set of interpolation functions for the neutrino flux at Earth due to annihilation in the Sun, for a range of DM annihilation channels, and includes the effects of electroweak corrections. The code takes into account

⁴It is worth noting that the annihilation of *pairs* of DM pairs is implied by a possible \mathbb{Z}_2 symmetry that makes the DM candidate stable. Besides this, we comment that annihilation could be very suppressed in an asymmetric DM scenario, in which the conservation of the DM quantum number would require the annihilation of a DM particle and antiparticle.

the cascade of the primary annihilation products into neutrinos within the Sun, as well as the subsequent neutrino oscillation in the Sun, in vacuum, and within the Earth.

What matters, in particular, are the branching ratios (BR) of DM pairs into SM final states: once equilibrium is achieved, the neutrino flux at Earth depends only on the relative annihilation cross sections to SM particles. This property is particularly interesting from the phenomenological point of view, because in the computation of the branching ratios, interesting simplifications occur and even the excitement of a resonance may have only a modest impact on the neutrino flux (see Sections 3.4, 4 and Appendix A).

Since the flux and spectrum of neutrinos from WIMP annihilations depend upon the preferred annihilation channels of the WIMPs, these constraints have traditionally been provided for extreme scenarios of WIMPs annihilating 100% into W^+W^- or $\tau^+\tau^-$, ‘hard’ channels corresponding to many high energy neutrinos and consequently a very stringent bound on the σ_{xp}^{SD} , or $b\bar{b}$, a ‘soft’ channel producing a very weak bound on σ_{xp}^{SD} [8]. These results can be recast for the scenario of known annihilation channels by the following method. The search utilizes the Unbinned Maximum Likelihood ratio method [61, 62], for which the sensitivity improves as $\text{Signal}/\sqrt{\text{Background}}$. For an unbinned maximum likelihood search of variable resolution, the background level varies as Ψ^2 where Ψ is the median angular resolution [63]. For a given differential (anti)-muon neutrino flux $\mathcal{F}(E)$, the total number of signal events expected within a sample can be calculated as

$$n_s(\mathcal{F}) = \int_{E_{\text{threshold}}}^{m_{\text{DM}}} \mathcal{F}(E) \times A_{\text{eff}}(E) dE, \quad (3.6)$$

where A_{eff} is the effective area from Fig. 3 of Ref. [62]. Since the fluxes and effective areas of ν_μ and $\bar{\nu}_\mu$ are different, Eq. 3.6 has to be evaluated separately for ν_μ and $\bar{\nu}_\mu$. The median energy $E_{\text{med}}(\mathcal{F})$ is then defined through

$$\int_{E_{\text{threshold}}}^{E_{\text{med}}} \mathcal{F}(E) \cdot A_{\text{eff}}(E) dE = \int_{E_{\text{med}}}^{m_{\text{DM}}} \mathcal{F}(E) \cdot A_{\text{eff}}(E) dE. \quad (3.7)$$

If the capture and annihilation processes in the Sun are in equilibrium, the neutrino flux, the capture/annihilation rate, as well as WIMP-nucleon scattering cross section all scale linearly with respect to each other. Thus the theoretical limit on the WIMP-nucleon scattering cross-section for a given flux prediction $\mathcal{F}_{\text{theory}}$ can be derived as

$$\sigma_{\text{theory}} = \sigma_{\text{benchmark}} \cdot \frac{n_s(\mathcal{F}_{\text{benchmark}})}{n_s(\mathcal{F}_{\text{theory}})} \cdot \frac{\Psi(E_{\text{med}}(\mathcal{F}_{\text{theory}}))}{\Psi(E_{\text{med}}(\mathcal{F}_{\text{benchmark}}))} \quad (3.8)$$

where the first term in the RHS accounts for the variation in the level of signal events while the second term accounts for the variation in background due to the shift in median angular resolution. An analogous scaling relation can also be used to obtain theoretical limits on the annihilation rate Γ_{ann} .

The bounds on Γ_{ann} for the IceCube benchmark channels can be derived from the limits on σ by mean of the tools provided by WimpSim and DarkSUSY.

The IceCube limit on the neutrino flux $\mathcal{F}_{\text{limit}}$ requires knowledge of the neutrino spectrum per annihilation as it would be observed at Earth. The first step is to calculate the branching ratio to all relevant final states. Results are discussed in Sec. 3.4.

In order to convert these branching ratios into the required neutrino spectrum, we use the PPPC 4 DM ID code. This is combined with the results for the branching ratios to determine the final spectrum of muon neutrinos and antineutrinos per DM annihilation event. The Zh , γh and γZ final states are not available in the code, and so we use the average of the two pair-production spectra for each of these final states. We assume that the differences in the kinematical distributions, due to the different masses of Z , h and γ , have a minor impact on the shape of the final neutrino flux.

For the theoretical flux prediction thus obtained, the number of expected signal events as well as the median energy can be obtained from the expressions in Eqs. (3.6) and (3.7) for each of the three IceCube samples described in Ref. [62]. The integrals are evaluated separately for ν_μ and $\bar{\nu}_\mu$. These quantities can also be evaluated for the IceCube benchmark channel flux predictions ($\mathcal{F}_{\text{benchmark}}$) obtained from WimpSim 3.03 and nusigma 1.17. Subsequently, theoretical limits on σ and Γ_{ann} can be obtained using the scaling relation (3.8) and the analogous one for Γ_{ann} .

For a given $\mathcal{F}_{\text{theory}}$, σ_{theory} can be calculated w.r.t any of the three benchmark IceCube channels. The different calculations are consistent to within $\sim 30\%$ and are thus averaged.

3.4 Results for the Branching Ratios

As discussed in the previous section, in order to extract bounds from IceCube observations, the branching ratios for the annihilations of DM pairs into SM final states must be computed. In this section we present the final results for the BR's, based on the cross sections that are computed in detail in Appendix A.

Fig. 4 shows the BR's into SM two-body final states as a function of m_χ , for $m_{Z'} = 10$ TeV and for six different values of θ (defined in Eq. (2.3)). The BR's for the final states shown on the plots do not depend at all on $g_{Z'}$ and g_χ , because they cancel in the ratios of cross sections, as can be seen from the formulæ in Appendix A. Leaving aside for a moment the pure $U(1)_{B-L}$, the main annihilation channels are the heavy fermion pairs ($t\bar{t}$, $b\bar{b}$ and $\tau^+\tau^-$) and Zh . These are indeed the only tree level channels for which $a \not\approx 0$ in the low velocity expansion $\sigma v_{\text{DM}} \sim a + b v_{\text{DM}}^2$.

The main annihilation channel below the kinematic threshold $m_\chi = 108$ GeV for Zh production is $b\bar{b}$, while the BR's into $c\bar{c}$ and $\tau^+\tau^-$ are less than 10% each. Even if its branching ratio is not the dominant one, the $\tau^+\tau^-$ channel dominates the IC bound below the Zh threshold because it yields more energetic neutrinos than the $b\bar{b}$ one.

In the region $m_\chi \sim 80$ GeV \div 108 GeV annihilation into W^+W^- may overcome the one into $b\bar{b}$, depending on the value of θ . Notice that, as will be explained at the end of this section, the one loop contribution to the W^+W^- cross section dominates over the tree level one, which is suppressed by the small $Z - Z'$ mixing angle and by the fact that, in the low velocity expansion, it has $a = 0$.

When the Zh channel opens up it overcomes all others and remains the only relevant channel unless $m_\chi \gtrsim m_{\text{top}}$, where the cross section into $t\bar{t}$ is comparable to the one to Zh . At higher DM masses, the cross section to Zh in the low v_{DM} limit is proportional to m_χ^2 , while $\sigma(\chi\chi \rightarrow t\bar{t})$ is basically constant in m_χ . The former proportionality comes from the final state with a longitudinally polarised Z boson and a Higgs boson, and is ultimately

due to the derivative coupling of would-be Goldstone bosons. This explains why Zh is the only relevant channel at large m_χ .

Around the resonance $\sigma(\chi\chi \rightarrow Zh)$ goes to 0 because the coefficient a in the low velocity expansion $\sigma v_{\text{DM}} \sim a + b v_{\text{DM}}^2$ vanishes. The reason is explained in Appendix A. Therefore, in a small window around the resonance, other channels dominate. The position of this window is basically the only way in which the branching ratios depend on $m_{Z'}$, as can be seen from Figs. 5 and 6.

The previous picture applies for all values of θ , except $\theta = \pi/2$ which corresponds to the pure $U(1)_{B-L}$ case. In that case, there is no mixing between Z and Z' , and the channel Zh disappears at tree level. Below the W^+W^- threshold $m_{\text{DM}} = m_W$, annihilation predominantly happens at tree level into fermionic channels. For $m_\chi > m_W$ the dominant channel is instead W^+W^- , with a $\mathcal{O}(10\%)$ contribution from ZZ . Annihilation into these channels is due to a diagram with a triangular fermionic loop, as discussed in Appendix A. The fermion channels, in the zero velocity limit, have a cross section proportional to $m_f^2 c_f^A{}^2$, where m_f is the fermion mass and c_f^A is the coupling of Z' to the axial vector fermion bilinear. When $U(1)'$ is reduced to $U(1)_{B-L}$ the Z' couples to the vector current only. Thus in this limit the $\sigma(\chi\chi \rightarrow f\bar{f})$ has $a = 0$. The coefficient b is not proportional to m_f^2 (as it is a because of the helicity suppression), thus in the fourth plot of Fig. 4 the fermions contribute equally to the annihilation cross section (apart from a factor $B^2 \times (\# \text{ colours}) = 1/3$ which penalises quarks with respect to leptons), unlike what happens for $\theta \neq \pi/2$.

Let us conclude this section by explaining why the tree level contribution for $\chi\chi \rightarrow W^+W^-$ has $a = 0$, which, together with the additional suppression by $\sin\psi$, selects Zh as the main channel at low velocities. The initial state $\chi\chi$, in the limit $v_{\text{DM}} \rightarrow 0$, has total angular momentum $J = 0$ and CP eigenvalue -1 . The final state Zh is not a CP eigenstate, unlike W^+W^- . Now, a pair of vector bosons can have a CP eigenvalue -1 and a total angular momentum $J = 0$ only if they are both transversally polarized [64]. In this case, the tree level interaction $Z'WW$ (2.8) turns out to give a vanishing cross section. We notice that this argument does not apply to the W^+W^- and ZZ amplitudes when the triangular fermion loop is included (see Fig. 7). In those cases, the effective $Z'W^+W^-$, $Z'ZZ$ vertices contain the terms

$$f_5^{Z'WW} \epsilon^{\mu\nu\rho\sigma} (k_1 - k_2)_\sigma Z'_\mu W_\nu^+ W_\rho^-, \quad f_5^{Z'ZZ} \epsilon^{\mu\nu\rho\sigma} (k_1 - k_2)_\sigma Z'_\mu Z_\nu Z_\rho, \quad (3.9)$$

where k_1, k_2 are the four-momenta of the outgoing bosons (see also [65, 66]). These terms lead to $a \neq 0$ in the cross section, making the W^+W^- and ZZ channels relevant despite of the loop suppression.

4 Summary of results

We show in Fig. 5 bounds on $\sigma_{\chi p}^{\text{SD}}$ for the case $\theta = 0$, comparing direct detection results with those coming from IceCube and LHC's mono-jet searches. Analogous results for different values of θ are presented in Fig. 6, in the plane Λ vs. m_χ . As representative values of θ we choose $\theta = 0, \pi/4, \pi/2$ and $3\pi/4$. We did not consider $\theta = \pi$ because it is exactly

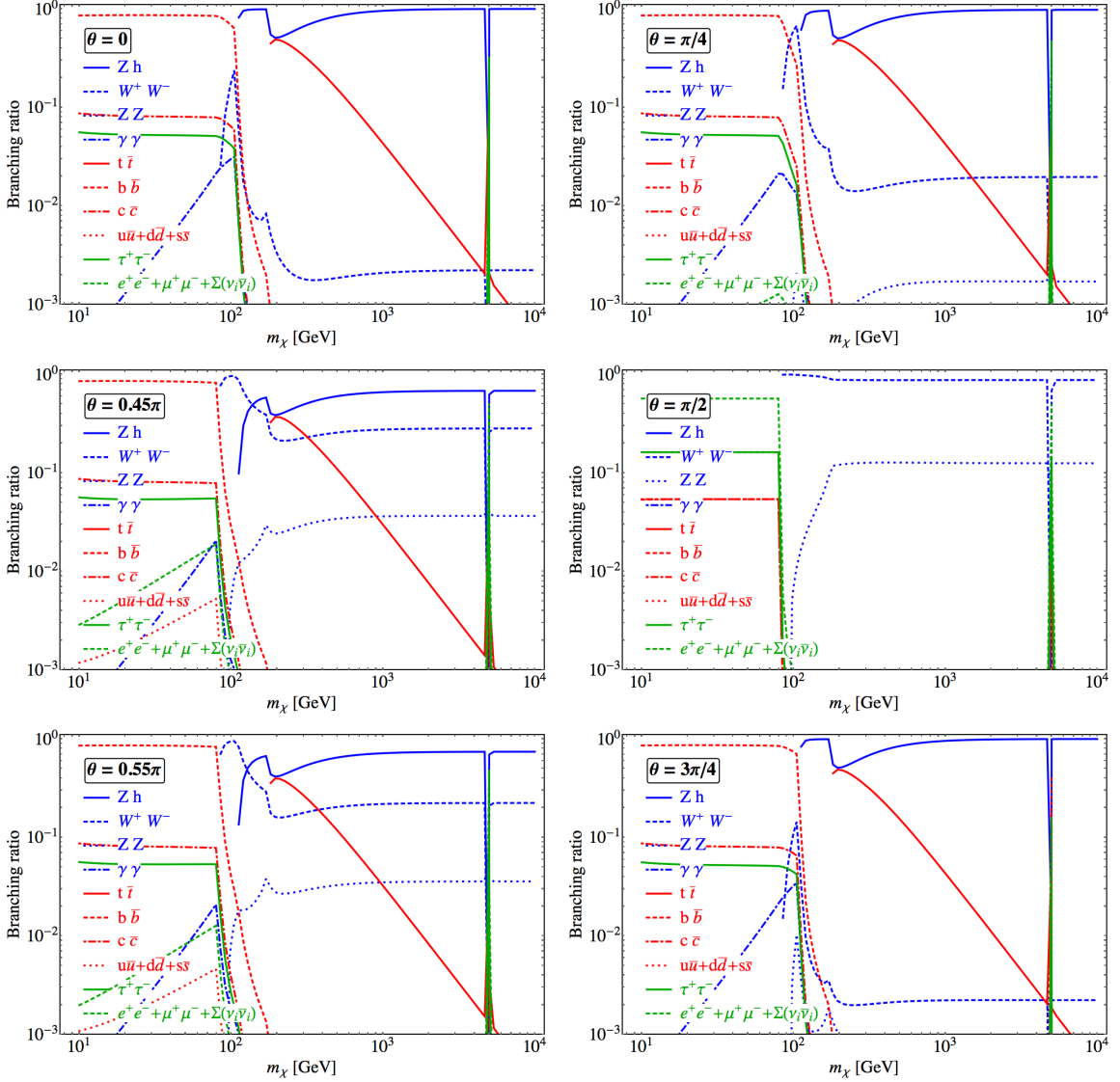


Figure 4. Branching ratios for the annihilation of $\chi\chi$ into pairs of SM particles, for $m_{Z'} = 10$ TeV and a kinetic energy of the DM particles equal to the thermal one in the Sun core. There is no dependence on $g_{Z'}$ and g_χ . The six plots, from left to right and top to bottom, correspond to $\theta = 0, \pi/4, 0.45\pi, \pi/2, 0.55\pi, 3\pi/4$. Only the channels with a BR greater than 10^{-3} are shown.

equivalent to $\theta = 0$. Since $\theta = \pi/2$ is quite a peculiar point, we added two values of θ in its vicinity, namely 0.45π and 0.55π .

As is clear from Eq. 3.3 and Table 2, for a generic angle θ the DM-nucleon scattering is mediated by a linear combination of $\mathcal{O}_4, \mathcal{O}_8$ and \mathcal{O}_9 , with coefficients similar in magnitude. The contributions from \mathcal{O}_8 and \mathcal{O}_9 can be safely ignored for IceCube: given the composition of the solar environment, their nuclear form factors are between 100 and 1000 times smaller than the one for \mathcal{O}_4 [67]. This is not the case for DD experiments, where the three operators give a similar contribution, and the scattering cross section is not exactly $\sigma_{\chi p}^{\text{SD}}$, which is

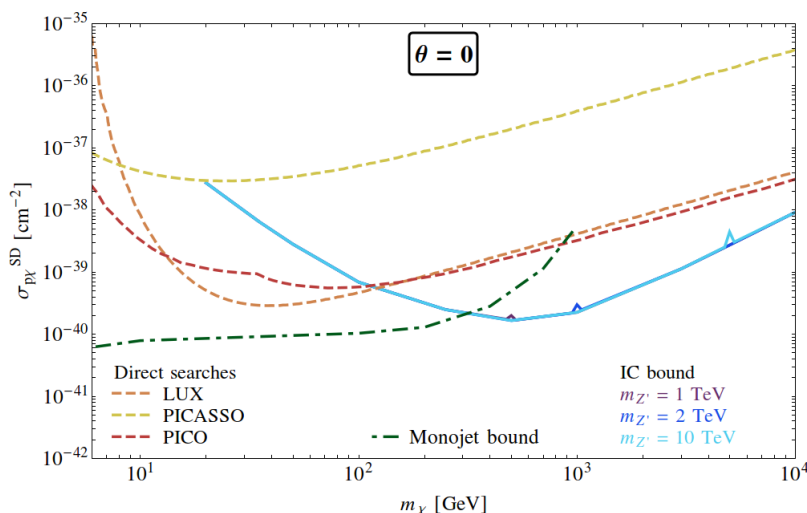


Figure 5. Bound on $\sigma_{\chi p}^{\text{SD}}$ from direct detection, LHC’s monojet analysis, and IceCube, for $\theta = 0$.

defined as being given by the operator \mathcal{O}_4 alone.

To obtain a bound in the usual $\sigma_{\chi p}^{\text{SD}}$ vs. m_χ plane, one needs to first obtain a bound on the total scattering cross section, which is easily done using the results of [53]. Then, this bound is translated into a bound on $\Lambda = m_{Z'}/(g_{Z'}\sqrt{g_\chi})$, using the expression for the cross section obtained from Eq. 3.1. Finally, the bound on Λ is translated into a bound on $\sigma_{\chi p}^{\text{SD}}$ using the expression

$$\sigma_{\chi p}^{\text{SD}} = \frac{3}{\pi} \left(-\frac{c_4}{\Lambda^2} \right)^2 \mu_p^2 \quad (4.1)$$

which gives the scattering cross section when only the \mathcal{O}_4 operator is involved, where μ_p is the reduced mass of the proton–DM system, and the dimensionless coefficient is given by $c_4 = \frac{1}{4} \cos\theta(\Delta_u - \Delta_d - \Delta_s) \simeq \frac{1}{4} \cos\theta \cdot 1.35$, with Δ_q parametrizing the quark spin content of each nucleon, and is assumed to be equal for protons and neutrons [53].

For $\theta \neq 0$, we do not show bounds on $\sigma_{\chi p}^{\text{SD}}$ but only on Λ . The reason is that, since $\sigma_{\chi p}^{\text{SD}}$ is defined as the contribution to the scattering cross section due to the operator \mathcal{O}_4 only, given the limit on Λ we have $\sigma_{\chi p}^{\text{SD}} \propto \cos^2\theta/\Lambda_{\text{lim}}^4$. When θ gets close to $\pi/2$, the computed value of $\sigma_{\chi p}^{\text{SD}}$ goes to 0 independently of Λ_{lim} , resulting in a spuriously strong bound.

The situation is slightly different when $\theta = \pi/2$. In this case, the coupling of the Z' to the vectorial current of the quark fields is identically 0, and therefore the coefficient of the \mathcal{O}_4 operator in the NR expansion vanishes. While for IceCube the contribution of \mathcal{O}_9 is subdominant with respect to that of \mathcal{O}_8 and can be ignored, both of them have to be taken into account to obtain DD bounds. A recast of the bound on Λ in terms of the usual $\sigma_{\chi p}^{\text{SD}}$ would make no sense in this scenario.

The PICO experiment gives interesting direct detection bounds. For $\theta = 0$ (*i.e.* for the usual spin-dependent operator \mathcal{O}_4), bounds on $\sigma_{\chi p}^{\text{SD}}$ can be read directly from Ref. [5], and translated into a bound on Λ . Bounds on Λ for other values of θ can not be obtained following the procedure we adopted for the other experiments, because PICO is not yet

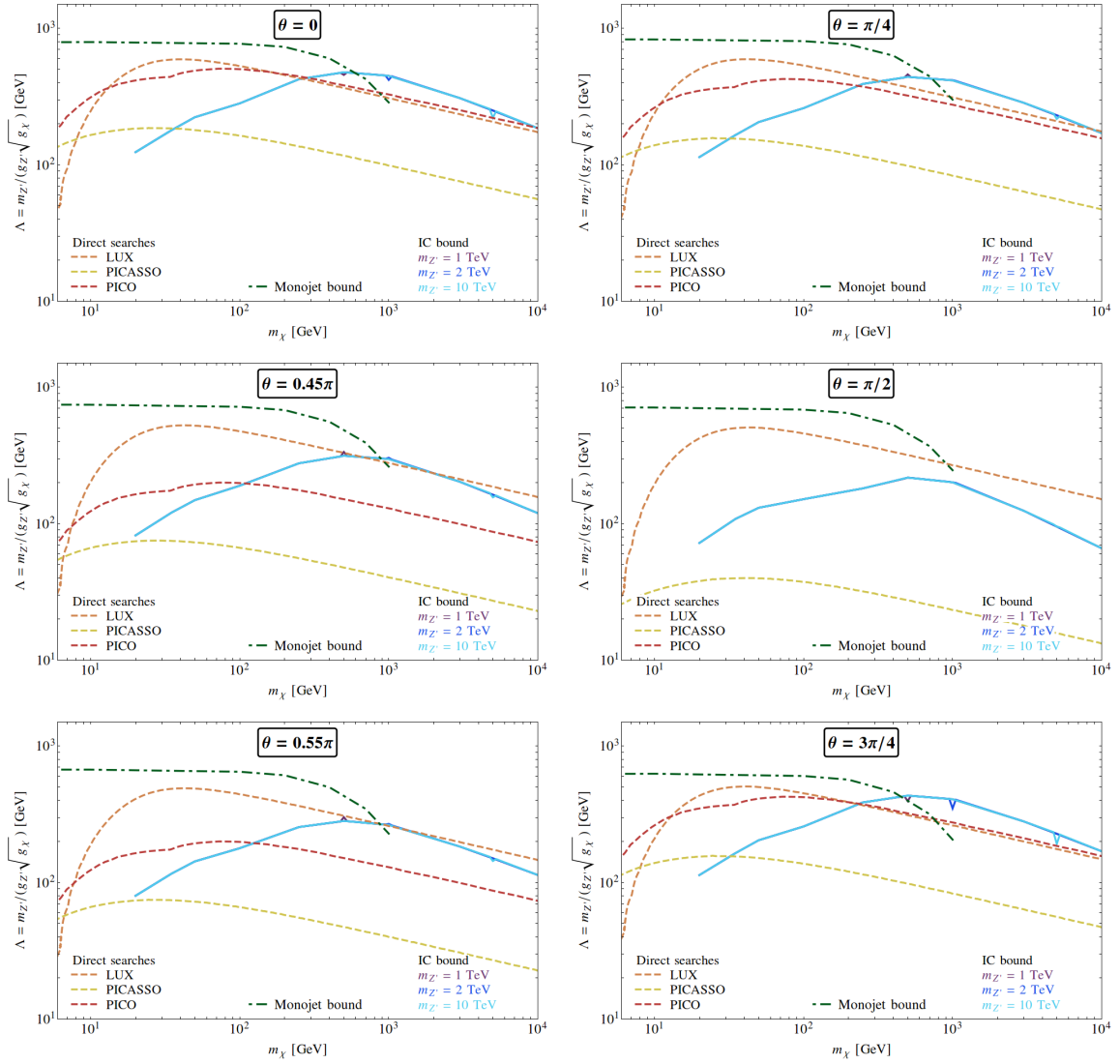


Figure 6. Bound on $\Lambda = m_{Z'}/(g_{Z'}\sqrt{g_\chi})$ from direct detection, LHC’s monojet analysis, and IceCube, for different values of θ .

included between the Test Statistic functions given in [53]. Therefore, we obtained a conservative bound on Λ by rescaling the PICO limit on $\sigma_{\chi p}^{\text{SD}}$ as $\cos^2\theta$ (since this enters the coefficient of the \mathcal{O}_4 operator) and then applying Eq. (4.1).

Let us now comment briefly on the results shown in Figs. 5 and 6. Bounds coming from LHC searches are typically the strongest ones in the low mass region, up to $m_\chi \sim 400 \div 700$ GeV for large θ . IceCube searches have their maximal sensitivity in the region between a few hundred GeV and a few TeV. When θ is small, in this mass region they give the strongest constraint on Λ . In particular, for $\theta = 0$ the constraint from IceCube is the dominant one from $m_\chi \sim 100$ GeV up to 10 TeV and beyond.

We notice that the bounds shown in Fig. 6 fall in the region where the DM is under-abundantly produced via the freeze-out mechanism (compare with Fig. 2). The difference

between the two values of Λ goes up to one order of magnitude for large m_χ .

An important remark about IceCube results is that they are almost independent of $m_{Z'}$ and $\Gamma_{Z'}$ (together with $g_{Z'}$, g_χ , as stressed in Sec. 3.4). There are two reasons for this: first, as explained previously, when the equilibrium between annihilation and capture in the Sun is reached, neutrino fluxes at Earth only depend on branching ratios, which are not modified dramatically by the resonance except for a very narrow region around it. Electroweak corrections further dilute the difference, and as a result IceCube bounds for different values of $m_{Z'}$ are almost superimposed (except for a small bump around the resonant point, whose width is $\sim \Gamma_{Z'}$).

Previous studies of the constraints coming from the IceCube experiment were done in Refs. [68, 69]. In these works, the authors examined simplified models without considering the mixing of Z and Z' imposed by the Higgs boson charge under $U(1)'$, and therefore they do not include annihilation channels which turn out to be the dominant ones. Moreover, they weight the nominal IceCube benchmarks (which assume 100% annihilation into one channel) by the annihilation cross sections into different channels computed in their model, and they do not take into account EW corrections. In our work, we compute the BR's into various SM channels in a complete and consistent model, and we compute the neutrino fluxes including the EW corrections with the help of PPC4DM ID. We infer the exclusion bounds with a recast of IceCube limits, as explained in Sec. 3.3, using the full shape of the neutrino fluxes to obtain the new bound.

5 Conclusions

While the spin-independent WIMP scenario has been probed experimentally to very high precision and direct detection experiments basically disfavor this possibility, the bounds on SD DM are much milder. WIMP-strength interactions between spin-dependent DM and baryonic matter are still perfectly allowed. Moreover, often the strongest bounds on SD DM do not come from direct detection experiments, but rather from LHC searches (direct or indirect) and IceCube.

In this work we analyzed and compared these constraints, coming from different experiments. In order to be concrete, we concentrated on a particular set of spin-dependent DM models, in which the DM-baryon interaction is mediated by a heavy gauge Z' . If we restrict ourself to the models without spectators at the EW scale, the parameter space of gauge Z' models can be conveniently parametrized by three quantities: the mass of the heavy Z' , the gauge coupling and the mixing angle θ between the hypercharge and $U(1)_{B-L}$ generators.

Although this study is not completely generic, as it does not cover all possible consistent models of SD DM, there are good reasons to believe that these models capture important phenomenological features that are generic to WIMP-like SD DM. We identified the region of parameter space favored by the observed thermal relic abundance and we have reanalyzed the existing LHC constraints, both direct (from the monojet searches) and indirect, on the Z' mass and coupling.

More importantly, we fully analyzed the low-temperature annihilation branching ratios of the Z' -mediated DM, which is crucial to derive IceCube constraints. In order to properly understand the expected neutrino fluxes from DM annihilation in the Sun's core, one has to know the annihilation channels of the DM in the Sun. Simply assuming that the dominant expected source of neutrinos is the WW or $b\bar{b}$ channel (as is done in the IceCube papers) is clearly insufficient. We found that, depending on the DM mass, one can divide the parameter space into three different regions. Below the Zh mass threshold (very light DM) the annihilations are indeed dominated by the $b\bar{b}$ channel, yielding very soft neutrino fluxes, although even in this case the IceCube constraints are dominated by small branching ratio to $\tau^+\tau^-$. Above this threshold Zh is a dominant annihilation channel and the dominant source of neutrinos almost in the entire parameter space. The third region is just above the $t\bar{t}$ mass threshold. If the DM mass sits in this “island”, one usually gets comparable annihilations into Zh and $t\bar{t}$, and both should be taken into account for the neutrino flux calculations. The W^+W^- channel can also become important, or even the leading channel, if the $U(1)'$ extension is very close to being $U(1)_{B-L}$. In this work we have properly recast the existing IceCube bounds including electroweak corrections, in order to derive reliable exclusion bounds on the secondary neutrinos coming from all annihilation channels.

We find that currently the strongest bounds on the SD Z' -mediated DM are imposed by LHC searches (for $m_{DM} \lesssim 400$ GeV) and by IceCube for heavier DM candidates, which are favored by thermal relic considerations. We also find that the best direct detection bounds come mostly from LUX (PICO becomes dominant only for very light ~ 20 GeV DM particles). These bounds are subdominant with respect to LHC ones in the case of light DM, but can be comparable to IC bounds for heavy DM if $U(1)'$ is close to being a $U(1)_{B-L}$ extension. We have also computed the values that yield the observed DM abundance through the freeze out mechanism, and we found that experimental exclusion limits fall in the slightly underabundant region.

Finally we notice that it would be interesting to see similar works for other SD DM candidates. It would be also useful to have bounds on the DM, annihilating into Zh reported directly by the IC collaboration. We stress that this channel immediately arises when considering a consistent anomaly-free model for a $U(1)'$ extension which is not a pure $U(1)_{B-L}$. This important feature is not captured by the use of so-called simplified models if these issues are not considered.

Acknowledgments

We thank Maxim Perelstein, Stefan Pokorski, Sofia Vallecorsa for discussions. D.R. and A.R. are supported by the Swiss National Science Foundation (SNSF), project “Investigating the Nature of Dark Matter” (project number: 200020.159223). A.K. is grateful to the organizers of KITP program “Experimental Challenges for the LHC run II” where this paper has been partially completed (partially supported by National Science Foundation under Grant No. NSF PHY11-25915).

A Details of the annihilation rate calculation

In this appendix we present the calculation of the annihilation cross sections of the DM into the SM in detail. We also go in detail over the one-loop order annihilation into the WW . The results of this calculations are summarized on Fig. 4

The Feynman diagrams for the possible annihilation channels of $\chi\chi$ into the SM particles are shown on Fig. 7. For each channel, we consider the leading order (tree level or one-loop), moreover we always restrict the calculation to the leading order in the mixing angle between Z and Z' , ψ .

At the tree level the DM annihilates into $f\bar{f}$, and if $\theta \neq \pi/2$ also to W^+W^- and Zh . Eqs. (A.1) to (A.6) summarize the annihilation cross sections into all these channels at the tree level, distinguishing between the polarization of the vector bosons in the final states through a superscript (T) or (L) for transverse or longitudinal polarization, respectively.

$$\sigma(\chi\chi \rightarrow f\bar{f}) = \frac{g_x^2 g_{Z'}^4 \cos^4 \psi N_c^f}{3\pi s((s - m_{Z'}^2)^2 + \Gamma_{Z'}^2 m_{Z'}^2)} \sqrt{\frac{s - 4m_f^2}{s - 4m_\chi^2}} \left((g_f^V)^2 (s - 4m_\chi^2)(s + 2m_f^2) + (g_f^A)^2 \left(s(s - 4m_\chi^2) + 4m_f^2 \left(m_\chi^2 \left(7 - 6\frac{s}{m_{Z'}^2} + 3\frac{s^2}{m_{Z'}^2} \right) - s \right) \right) \right), \quad (\text{A.1})$$

$$\begin{aligned} \sigma(\chi\chi \rightarrow Z^{(L)}h) &= g_x^2 g_{Z'}^4 \cos^2 \theta \cos^4 \psi \frac{\sqrt{(s - (m_h^2 + m_Z^2))^2 - 4m_h^2 m_Z^2}}{((s - m_{Z'}^2)^2 + \Gamma_{Z'}^2 m_{Z'}^2)} \frac{1}{48\pi s^{5/2}} \cdot \\ &\cdot \left(\left(m_h^4 (2m_\chi^2 + s) - 2m_h^2 (s + 2m_\chi^2)(s + m_Z^2) + 2m_\chi^2 (s^2 - 10sm_Z^2 + m_Z^4) + s(s + m_Z^2)^2 \right) \right. \\ &\quad \left. + \frac{1}{m_{Z'}^2} \left(-6m_\chi^2 s (m_h^4 - 2m_h^2 (m_Z^2 + s) + (m_Z^2 - s)^2) \right) \right. \\ &\quad \left. + \frac{1}{m_{Z'}^4} \left(3m_\chi^2 s^2 (m_h^4 - 2m_h^2 (s + m_Z^2) + (s - m_Z^2)^2) \right) \right), \quad (\text{A.2}) \end{aligned}$$

$$\sigma(\chi\chi \rightarrow Z^{(T)}h) = g_x^2 g_{Z'}^4 \cos^2 \theta \cos^4 \psi \frac{\sqrt{(s - (m_h^2 + m_Z^2))^2 - 4m_h^2 m_Z^2}}{((s - m_{Z'}^2)^2 + \Gamma_{Z'}^2 m_{Z'}^2)} \frac{m_Z^2 (s - 4m_\chi^2)^{1/2}}{6\pi s^{3/2}}, \quad (\text{A.3})$$

$$\begin{aligned} \sigma(\chi\chi \rightarrow W^{+(L)}W^{-(L)}) &= g_x^2 g_{Z'}^4 \alpha_W \cos^2 \theta_W \cos^2 \psi \sin^2 \psi (s - 4m_W^2)^{3/2} (s - 4m_\chi^2)^{1/2} \cdot \\ &\cdot \frac{(m_{Z'}^2 - m_Z^2)^2 + (\Gamma_{Z'} m_{Z'} - \Gamma_Z m_Z)^2}{((s - m_{Z'}^2)^2 - \Gamma_{Z'}^2 m_{Z'}^2)((s - m_Z^2)^2 - \Gamma_Z^2 m_Z^2)} \frac{(2m_W^2 + s)^2}{12m_W^4 s}, \quad (\text{A.4}) \end{aligned}$$

$$\begin{aligned} \sigma(\chi\chi \rightarrow W^{\pm(T)}W^{\mp(L)}) &= g_x^2 g_{Z'}^4 \alpha_W \cos^2 \theta_W \cos^2 \psi \sin^2 \psi (s - 4m_W^2)^{3/2} (s - 4m_\chi^2)^{1/2} \cdot \\ &\cdot \frac{(m_{Z'}^2 - m_Z^2)^2 + (\Gamma_{Z'} m_{Z'} - \Gamma_Z m_Z)^2}{((s - m_{Z'}^2)^2 - \Gamma_{Z'}^2 m_{Z'}^2)((s - m_Z^2)^2 - \Gamma_Z^2 m_Z^2)} \frac{4}{3m_W^2}, \quad (\text{A.5}) \end{aligned}$$

$$\begin{aligned} \sigma(\chi\chi \rightarrow W^{+(T)}W^{-(T)}) &= g_x^2 g_{Z'}^4 \alpha_W \cos^2 \theta_W \cos^2 \psi \sin^2 \psi (s - 4m_W^2)^{3/2} (s - 4m_\chi^2)^{1/2} \cdot \\ &\cdot \frac{(m_{Z'}^2 - m_Z^2)^2 + (\Gamma_{Z'} m_{Z'} - \Gamma_Z m_Z)^2}{((s - m_{Z'}^2)^2 - \Gamma_{Z'}^2 m_{Z'}^2)((s - m_Z^2)^2 - \Gamma_Z^2 m_Z^2)} \frac{2}{3s}. \quad (\text{A.6}) \end{aligned}$$

A few clarifications are in order about the annihilation cross sections of the DM at tree level.

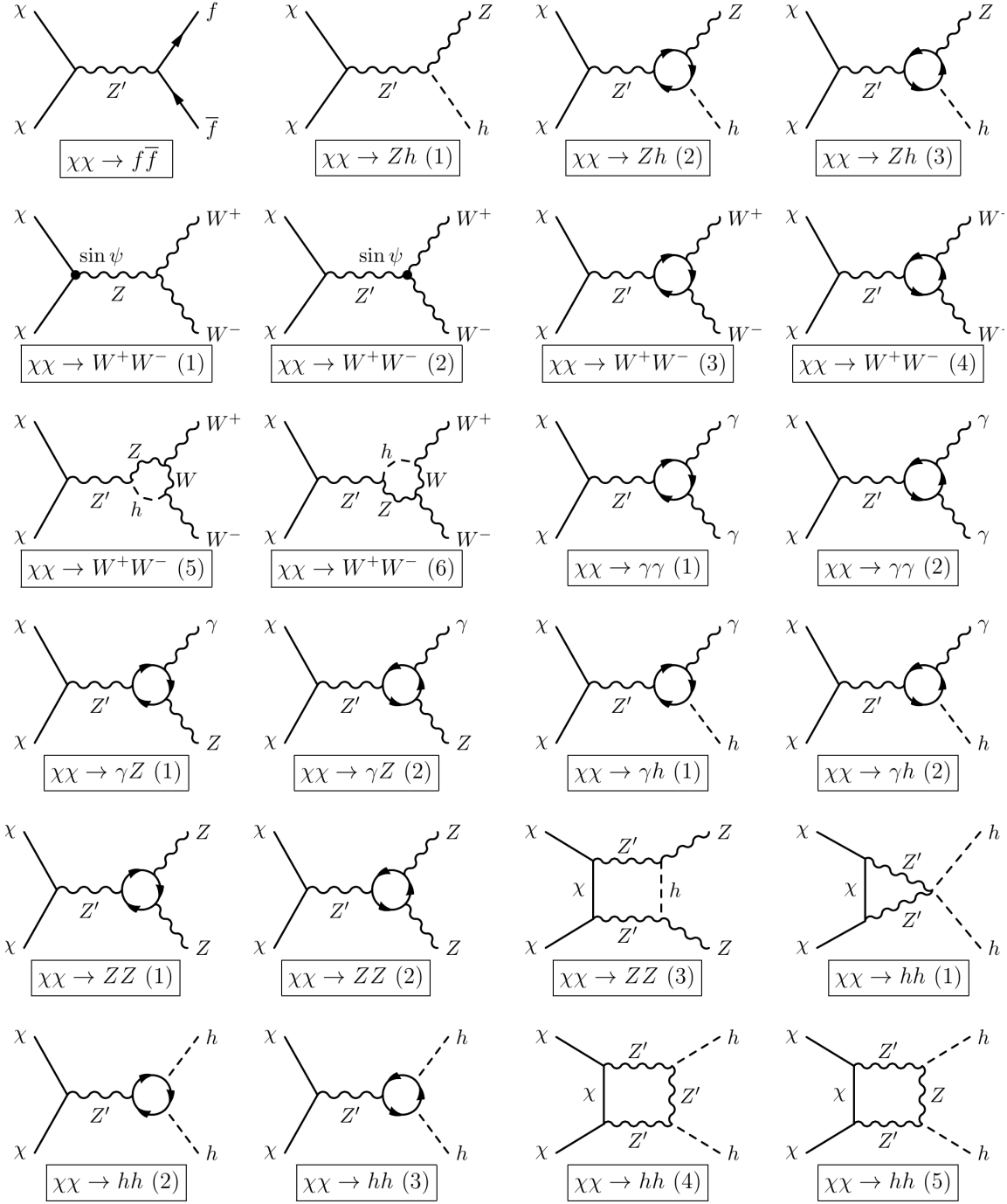


Figure 7. Feynman diagrams for the annihilation of $\chi\chi$ into pairs of SM particles that have been considered in this work. In the fermion loops, the amplitude is summed over all the SM fermions.

$f\bar{f}$: We denote the number of colors of the fermion f by N_c^f , and its vector and axial vector couplings to Z' by g_f^V, g_f^A respectively. The values of g_f^V, g_f^A are given in Tab. 2. In the zero velocity limit, corresponding to $s = 4m_\chi^2$, the cross section is proportional to m_f^2 , because of the helicity suppression for pairs of annihilating fermions. In

that limit, $\sigma \propto (g_f^A)^2 \propto \cos^2 \theta$, i.e. the a coefficient in the low velocity expansion $\sigma v \simeq a + bv^2$ comes from the $U(1)_Y$ component of the $U(1)'$ extension.

Zh: The diagram on Fig. 7 contains the tree level vertex $Z'Zh$ of Eq. (2.7). In the zero velocity limit, the only contribution comes from the production of a longitudinally polarized Z , since in Eq. (A.3) the factor $(s - 4m_\chi^2)^{1/2}$ vanishes.

WW: We denote $\alpha_W = g_W^2/(4\pi)$, where g_W is the weak coupling constant. The amplitude is the sum of the two diagrams on Fig. 7: the annihilation occurs via the mixing of Z and Z' and the SM trilinear gauge vertex ZWW , see Eq. (2.8). For each of the final polarization states, the cross section is proportional to $(s - 4m_\chi^2)^{1/2}$.

Given that $\sigma(\chi\chi \rightarrow WW)v_{\text{DM}}$ (where v_{DM} is the DM velocity) is suppressed by $\sin^2 \psi$ and by v_{DM}^2 at tree level it is worth checking whether contributions arising at one loop can become important. The contribution to the amplitude of diagrams 5 and 6 on Fig. 7 is velocity suppressed because of the same argument reported at the end of Sec. 3.4. Therefore we only considered the contribution to the cross section coming from the sum of diagrams 3 and 4, also ignoring the interference terms with the other diagrams.

We also computed the cross sections for the annihilations into ZZ , $\gamma\gamma$, γh , γZ and hh at one loop. It is worth computing these corrections because of the velocity suppression of some tree level channels, and because in the pure $U(1)_{B-L}$ case the tree level annihilations into WW and Zh disappear. As for the Zh channel, we computed the one loop cross section only in the pure $U(1)_{B-L}$ case ($\theta = \pi/2$), in which the tree level amplitude vanishes, and the only remaining contribution comes from diagrams 2 and 3 in Fig. 7. The results of the loop calculation are:

$$\begin{aligned} \sigma(\chi\chi \rightarrow W^{+(T)}W^{-(T)}) &= \frac{g_Z^4 g_\chi^2 N_c^i (s - 4m_W^2)^{3/2} \alpha_W^2}{768\pi^3 \left(\Gamma_{Z'}^2, m_{Z'}^2 + (m_{Z'}^2 - s)^2 \right) s \sqrt{s - 4m_\chi^2}} \\ &\cdot \left\{ \frac{48m_\chi^2 (s - m_{Z'}^2)^2}{m_{Z'}^4 (s - 4m_W^2)^2} \left| \sum_i N_c^i \left\{ (g_{d^i}^L - g_{d^i}^R) B_0(s, m_{d^i}^2, m_{d^i}^2) m_{d^i}^2 - \right. \right. \right. \\ &- (g_{d^i}^L - g_{d^i}^R) (m_{d^i}^2 - m_{u^i}^2 - m_W^2) C_0(m_W^2, m_W^2, s, m_{d^i}^2, m_{u^i}^2, m_{d^i}^2) m_{d^i}^2 - \frac{1}{2} (g_{d^i}^L + g_{u^i}^L) (s - 4m_W^2) + \\ &+ \left. \left. \left. \left((g_{d^i}^R - g_{u^i}^L) m_{d^i}^2 + (g_{u^i}^R - g_{u^i}^L) m_{u^i}^2 \right) B_0(m_W^2, m_{d^i}^2, m_{u^i}^2) + (g_{u^i}^L - g_{u^i}^R) m_{u^i}^2 B_0(s, m_{u^i}^2, m_{u^i}^2) + \right. \right. \right. \\ &\left. \left. \left. + (g_{u^i}^L - g_{u^i}^R) m_{u^i}^2 (m_{d^i}^2 - m_{u^i}^2 + m_W^2) C_0(m_W^2, m_W^2, s, m_{u^i}^2, m_{d^i}^2, m_{u^i}^2) \right\} \right|^2 \\ &+ \frac{32}{81} \frac{s - 4m_\chi^2}{m_W^4 (s - 4m_W^2)^4} \left| \sum_i N_c^i \left\{ \frac{1}{2} (s - 4m_W^2) ((3m_{d^i}^2 - 3m_{u^i}^2 + 7m_W^2 - 5s/2) g_{d^i}^L + \right. \right. \right. \\ &+ (3m_{d^i}^2 - 3m_{u^i}^2 - 7m_W^2 + 5s/2) g_{u^i}^L) m_W^2 + \frac{3}{2} \left[3g_{d^i}^R (s - 4m_W^2) m_{d^i}^2 + g_{d^i}^L (-6m_{d^i}^4 + 2(6m_{u^i}^2 + 2m_W^2 + s) m_{d^i}^2 - \right. \\ &- 6m_{u^i}^4 + 6m_W^4 + s^2 - 3m_{u^i}^2 s - 7m_W^2 s) \left. \right] B_0(s, m_{d^i}^2, m_{d^i}^2) m_W^2 - \frac{3}{2} \left[3g_{u^i}^R (s - 4m_W^2) m_{u^i}^2 + \right. \\ &+ g_{u^i}^L (-6m_{d^i}^4 - 3(s - 4m_{u^i}^2) m_{d^i}^2 - 6m_{u^i}^4 + 6m_W^4 + s^2 - 7m_W^2 s + 2m_{u^i}^2 (s + 2m_W^2)) \left. \right] B_0(s, m_{u^i}^2, m_{u^i}^2) m_W^2 - \\ &- \frac{9}{2} (m_W^2 - m_{d^i}^2 + m_{u^i}^2) \left[-g_{d^i}^R (s - 4m_W^2) m_{d^i}^2 + g_{d^i}^L (2m_{d^i}^4 - (s + 4m_{u^i}^2) m_{d^i}^2 + \right. \\ &\left. \left. + 2(m_{u^i}^4 + (s - 2m_W^2) m_{u^i}^2 + m_W^4)) \right] C_0(m_W^2, m_W^2, s, m_{d^i}^2, m_{u^i}^2, m_{d^i}^2) m_W^2 + \right. \end{aligned}$$

$$\begin{aligned}
& + 9 \left[-\frac{1}{2}(s - 4m_W^2)g_{u^i}^R m_{u^i}^2 + (m_{d^i}^4 + (s - 2m_{u^i}^2 - 2m_W^2)m_{d^i}^2 + m_{u^i}^4 + m_W^4 - m_{u^i}^2 s/2)g_{u^i}^L \right] \cdot \\
& \cdot (m_{d^i}^2 - m_{u^i}^2 + m_W^2)C_0(m_W^2, m_W^2, s, m_{u^i}^2, m_{d^i}^2, m_{u^i}^2)m_W^2 + \frac{3}{2}(m_{d^i}^2 - m_{u^i}^2)(g_{d^i}^L(m_{d^i}^2 - m_{u^i}^2 - m_W^2) - \\
& - g_{u^i}^L(m_{d^i}^2 - m_{u^i}^2 + m_W^2))(s - 4m_W^2)B_0(0, m_{d^i}^2, m_{u^i}^2) + 3 \left[-\frac{3}{2}(s - 4m_W^2)(g_{d^i}^R m_{d^i}^2 - g_{u^i}^R m_{u^i}^2)m_W^2 + \right. \\
& + g_{u^i}^L \left(\frac{1}{2}(m_{d^i}^4 - 2(m_{u^i}^2 + m_W^2)m_{d^i}^2 + m_{u^i}^4 + m_W^4 + m_{u^i}^2 m_W^2)s - m_W^2(5m_{d^i}^4 + 2(m_W^2 - 5m_{u^i}^2)m_{d^i}^2 + 5m_{u^i}^4 + \right. \\
& \left. + 5m_W^4 - 4m_{u^i}^2 m_W^2) \right) + g_{d^i}^L \left(m_W^2(5m_{d^i}^4 - 2(5m_{u^i}^2 + 2m_W^2)m_{d^i}^2 + 5m_{u^i}^4 + 5m_W^4 + 2m_{u^i}^2 m_W^2) - \right. \\
& \left. - \frac{1}{2}(m_{d^i}^4 + (m_W^2 - 2m_{u^i}^2)m_{d^i}^2 + (m_{u^i}^2 - m_W^2)^2)s \right) \left. \right] B_0(m_W^2, m_{d^i}^2, m_{u^i}^2) \left. \right\}^2 \quad (A.7)
\end{aligned}$$

We do not report the formula for $\sigma(\chi\chi \rightarrow W^{\pm(T)}W^{\mp(L)})$ because this channel turns out to have $a = 0$ (therefore it is irrelevant for the annihilation process in the Sun) and the corresponding formula is too cumbersome to be reported here.

$$\begin{aligned}
\sigma(\chi\chi \rightarrow W^{+(L)}W^{-(L)}) &= \frac{g_Z^4 g_\chi^2 \alpha_W^2 \sqrt{s - 4m_x^2}}{62208\pi^3 m_W^8 [(s - m_Z^2)^2 + \Gamma_Z^2 m_Z^2] s (s - 4m_W^2)^{5/2}} \cdot \\
& \cdot \left| \sum_i N_c^i \left\{ (4m_W^2 - s)m_W^2 \left(g_{u^i}^L (-4m_W^4 + 12m_{u^i}^2 m_W^2 + 2sm_W^2 - s^2 - 6m_{d^i}^2 (s - 2m_W^2)) \right. \right. \right. \\
& \quad \left. \left. - g_{d^i}^L (-4m_W^4 + 12m_{d^i}^2 m_W^2 + 2sm_W^2 - s^2 - 6m_{u^i}^2 (s - 2m_W^2)) \right) \right. \\
& \quad \left. + 6 \left(A_0(m_{d^i}^2) g_{d^i}^L - A_0(m_{u^i}^2) g_{u^i}^L \right) (s - 4m_W^2)^2 m_W^2 \right. \\
& - 3B_0(0, m_{d^i}^2, m_{u^i}^2) (m_{d^i}^2 - m_{u^i}^2) (4m_W^2 - s) \left(g_{u^i}^L (4m_W^4 - 2sm_W^2 + m_{u^i}^2 (8m_W^2 - s) + m_{d^i}^2 (s - 8m_W^2)) + \right. \\
& \quad \left. g_{d^i}^L (4m_W^4 - 2sm_W^2 + m_{d^i}^2 (8m_W^2 - s) + m_{u^i}^2 (s - 8m_W^2)) \right) \\
& + 3B_0(m_W^2, m_{d^i}^2, m_{u^i}^2) \left(6(g_{d^i}^R m_{d^i}^2 - g_{u^i}^R m_{u^i}^2) (4m_W^2 - s) m_W^4 + g_{d^i}^L [8m_W^8 + 12sm_W^6 - 2s^2 m_W^4 + \right. \\
& \quad (m_{d^i}^2 - m_{u^i}^2)^2 (32m_W^4 - 6sm_W^2 + s^2) + m_{u^i}^2 (8m_W^4 + 6sm_W^2 + s^2) m_W^2 + \\
& \quad \left. m_{d^i}^2 (-16m_W^6 - 12sm_W^4 + s^2 m_W^2) \right] - g_{u^i}^L [8m_W^8 + 12sm_W^6 - 2s^2 m_W^4 + \\
& (m_{d^i}^2 - m_{u^i}^2)^2 (32m_W^4 - 6sm_W^2 + s^2) + m_{u^i}^2 (-16m_W^4 - 12sm_W^2 + s^2) m_W^2 + m_{d^i}^2 (m_W^2 (8m_W^4 + 6sm_W^2 + s^2))] \left. \right) \\
& + 3B_0(s, m_{u^i}^2, m_{u^i}^2) m_W^2 \left(6g_{u^i}^R m_{u^i}^2 (4m_W^2 - s) m_W^2 + g_{u^i}^L [-24m_W^6 + 12sm_W^4 + 4s(s - 4m_{u^i}^2) m_W^2 + 6m_{d^i}^4 s \right. \\
& \quad \left. + s(6m_{u^i}^4 + sm_{u^i}^2 - s^2) + 3m_{d^i}^2 (8m_W^4 - 2sm_W^2 + s(s - 4m_{u^i}^2))] \right) \\
& - 3B_0(s, m_{d^i}^2, m_{d^i}^2) m_W^2 \left(6g_{d^i}^R m_{d^i}^2 (4m_W^2 - s) m_W^2 + g_{d^i}^L [-24m_W^6 + 12sm_W^4 + 4s(s - 4m_{d^i}^2) m_W^2 + 6m_{u^i}^4 s \right. \\
& \quad \left. + s(6m_{d^i}^4 + sm_{d^i}^2 - s^2) + 3m_{u^i}^2 (8m_W^4 - 2sm_W^2 + s(s - 4m_{d^i}^2))] \right) \\
& + 18C_0(m_W^2, m_W^2, s, m_{u^i}^2, m_{d^i}^2, m_{u^i}^2) m_W^2 \left(g_{u^i}^R m_{u^i}^2 (m_{d^i}^2 - m_{u^i}^2 + m_W^2) (4m_W^2 - s) m_W^2 \right. \\
& \quad \left. + g_{u^i}^L [sm_{d^i}^6 + (4m_W^4 - 2sm_W^2 + s(s - 3m_{u^i}^2)) m_{d^i}^4 + (-8m_W^6 + 5sm_W^4 + 3m_{u^i}^4 s \right. \\
& \quad \left. - m_{u^i}^2 (4m_W^4 + sm_W^2 + s^2)) m_{d^i}^2 - (m_{u^i}^2 - m_W^2) (4m_W^6 - 2m_{u^i}^2 sm_W^2 + m_{u^i}^4 s) \right) \\
& + 18C_0(m_W^2, m_W^2, s, m_{d^i}^2, m_{u^i}^2, m_{d^i}^2) m_W^2 \left(g_{d^i}^R m_{d^i}^2 (m_{d^i}^2 - m_{u^i}^2 - m_W^2) (4m_W^2 - s) m_W^2 \right. \\
& \quad \left. + g_{d^i}^L [-4m_W^8 + m_{d^i}^6 s - m_{u^i}^6 s - 3m_{d^i}^4 (m_{u^i}^2 + m_W^2) s + m_{u^i}^2 (8m_W^6 - 5m_W^4 s) \right.
\end{aligned}$$

$$- m_{u^i}^4 (4m_W^4 - 2sm_W^2 + s^2) + m_{d^i}^2 (3sm_{u^i}^4 + (4m_W^4 + sm_W^2 + s^2)m_{u^i}^2 + 2m_W^4(2m_W^2 + s)) \Bigg\} \Bigg|^2, \quad (\text{A.8})$$

$$\begin{aligned} \sigma(\chi\chi \rightarrow Z^{(T)} Z^{(T)}) &= \frac{4g_\chi^2 g_Z^4 m_\chi^2 m_Z^4 (m_{Z'}^2 - s)^2}{\pi^5 m_Z^4 s v^4 \sqrt{s - 4m_\chi^2} \sqrt{s - 4m_Z^2} (\Gamma_Z^2, m_Z^2, + (m_{Z'}^2 - s)^2)}. \\ &\cdot \left| \sum_f N_c^f \left\{ 4g_f^A m_Z^2 (c_f^L)^2 - 4g_f^V m_Z^2 (c_f^L)^2 - g_f^A s (c_f^L)^2 + g_f^V s (c_f^L)^2 + 4g_f^A (c_f^R)^2 m_Z^2 + 4(c_f^R)^2 g_f^V m_Z^2 \right. \right. \\ &- g_f^A (c_f^R)^2 s - (c_f^R)^2 g_f^V s - \left[g_f^A \left((4m_f^2 - 4m_Z^2 + s) (c_f^L)^2 - 8c_f^R m_f^2 c_f^L + (c_f^R)^2 (4m_f^2 - 4m_Z^2 + s) \right) \right. \\ &\quad \left. \left. + ((c_f^L)^2 - (c_f^R)^2) g_f^V (4m_Z^2 - s) \right] B_0(m_Z^2, m_f^2, m_f^2) + \left[((c_f^L)^2 - (c_f^R)^2) g_f^V (4m_Z^2 - s) \right. \right. \\ &\quad \left. \left. + g_f^A \left((4m_f^2 - 4m_Z^2 + s) (c_f^L)^2 - 8c_f^R m_f^2 c_f^L + (c_f^R)^2 (4m_f^2 - 4m_Z^2 + s) \right) \right] B_0(s, m_f^2, m_f^2) \right. \\ &\quad \left. \left. + 4g_f^A m_f^2 \left((c_f^L)^2 m_Z^2 + (c_f^R)^2 m_Z^2 + c_f^L c_f^R (2m_Z^2 - s) \right) C_0(s, m_Z^2, m_Z^2, m_f^2, m_f^2) \right\} \right|^2, \quad (\text{A.9}) \end{aligned}$$

$$\begin{aligned} \sigma(\chi\chi \rightarrow Z^{(T)} Z^{(L)}) &= \frac{4g_\chi^2 g_Z^4 m_Z^2 \sqrt{s - 4m_\chi^2}}{3\pi^5 s v^4 (s - 4m_Z^2)^{3/2} (\Gamma_Z^2, m_Z^2, + (m_{Z'}^2 - s)^2)}. \\ &\cdot \left| \sum_f N_c^f \left\{ -4g_f^A (c_f^L)^2 m_Z^4 - 4g_f^A (c_f^R)^2 m_Z^4 + 4(c_f^L)^2 g_f^V m_Z^4 - 4(c_f^R)^2 g_f^V m_Z^4 \right. \right. \\ &\quad \left. \left. + g_f^A (c_f^L)^2 s m_Z^2 + g_f^A (c_f^R)^2 s m_Z^2 - (c_f^L)^2 g_f^V s m_Z^2 + (c_f^R)^2 g_f^V s m_Z^2 \right. \right. \\ &\quad \left. \left. + \frac{1}{2} \left[g_f^A \left(- (20m_Z^4 - 6sm_Z^2 + s^2 + 4m_f^2(s - 4m_Z^2)) (c_f^L)^2 + 8c_f^R m_f^2 (s - 4m_Z^2) c_f^L \right. \right. \right. \right. \\ &\quad \left. \left. \left. - (c_f^R)^2 (20m_Z^4 - 6sm_Z^2 + s^2 + 4m_f^2(s - 4m_Z^2)) \right) \right] B_0(m_Z^2, m_f^2, m_f^2) \right. \right. \\ &\quad \left. \left. - \frac{1}{2} \left[g_f^A \left(- (20m_Z^4 - 6sm_Z^2 + s^2 + 4m_f^2(s - 4m_Z^2)) (c_f^L)^2 + 8c_f^R m_f^2 (s - 4m_Z^2) c_f^L \right. \right. \right. \right. \\ &\quad \left. \left. \left. - (c_f^R)^2 (20m_Z^4 - 6sm_Z^2 + s^2 + 4m_f^2(s - 4m_Z^2)) \right) \right] B_0(s, m_f^2, m_f^2) \right. \right. \\ &\quad \left. \left. + 2 \left[-\frac{1}{2} ((c_f^L)^2 - (c_f^R)^2) g_f^V \left(-2m_Z^6 + 2sm_Z^4 + m_f^2 (8m_Z^4 - 6sm_Z^2 + s^2) \right) \right. \right. \\ &\quad \left. \left. - \frac{1}{2} g_f^A \left((2m_Z^6 - 2sm_Z^4 + 4m_f^2 sm_Z^2 - m_f^2 s^2) (c_f^L)^2 + 2c_f^R m_f^2 (8m_Z^4 - 6sm_Z^2 + s^2) c_f^L \right. \right. \right. \\ &\quad \left. \left. \left. + (c_f^R)^2 (2m_Z^6 - 2sm_Z^4 + 4m_f^2 sm_Z^2 - m_f^2 s^2) \right) \right] C_0(s, m_Z^2, m_Z^2, m_f^2, m_f^2) \right\} \right|^2, \quad (\text{A.10}) \end{aligned}$$

$$\sigma(\chi\chi \rightarrow Z^{(L)}Z^{(L)}) = 0, \quad (\text{A.11})$$

$$\begin{aligned} \sigma(\chi\chi \rightarrow Z^{(T)}h)|_{\theta=\pi/2} &= \frac{\alpha_W g_\chi^2 g_{Z'}^4}{24\pi^4 (m_{Z'}^4 + \Gamma_{Z'}^2 m_{Z'}^2 - 2sm_{Z'}^2 + s^2)} \cdot \\ &\cdot \frac{\sqrt{s - 4m_\chi^2} \sqrt{(m_H^2 - m_Z^2)^2 + s^2 - 2s(m_H^2 + m_Z^2)}}{s^{3/2} v^2 ((m_H - m_Z)^2 - s)^2 ((m_H + m_Z)^2 - s)^2} \left| \sum_f g_f^V m_f^2 N_c^f (c_f^L + c_f^R) \cdot \right. \\ &\cdot \left\{ C_0(m_H^2, m_Z^2, s, m_f^2, m_f^2, m_f^2) s^3 + 2(-m_H^2 - m_Z^2 + s) B_0(s, m_f^2, m_f^2) s \right. \\ &- \left[2B_0(m_H^2, m_f^2, m_f^2) + (-4m_f^2 + 3m_H^2 + m_Z^2) C_0(m_H^2, m_Z^2, s, m_f^2, m_f^2, m_f^2) - 2 \right] s^2 \\ &+ \left[-2B_0(m_Z^2, m_f^2, m_f^2) m_Z^2 + 2(m_H^2 + 2m_Z^2) B_0(m_H^2, m_f^2, m_f^2) \right. \\ &- \left. \left. \left((8m_f^2 - 3m_H^2 + m_Z^2) C_0(m_H^2, m_Z^2, s, m_f^2, m_f^2, m_f^2) + 4 \right) (m_H^2 + m_Z^2) \right] s \right. \\ &- \left. (m_H^2 - m_Z^2) \left[-2B_0(m_H^2, m_f^2, m_f^2) m_Z^2 + 2B_0(m_Z^2, m_f^2, m_f^2) m_Z^2 \right. \right. \\ &\left. \left. + \left((-4m_f^2 + m_H^2 - m_Z^2) C_0(m_H^2, m_Z^2, s, m_f^2, m_f^2, m_f^2) - 2 \right) (m_H^2 - m_Z^2) \right] \right\} \Bigg|^2, \quad (\text{A.12}) \end{aligned}$$

$$\begin{aligned} \sigma(\chi\chi \rightarrow Z^{(L)}h)|_{\theta=\pi/2} &= \frac{\alpha_W g_\chi^2 g_{Z'}^4}{3\pi^4 (\Gamma_{Z'}^2 m_{Z'}^2 + m_{Z'}^4 - 2m_{Z'}^2 s + s^2)} \cdot \\ &\cdot \frac{m_Z^2 \sqrt{s - 4m_\chi^2}}{\sqrt{s} v^2 \left(-2s(m_H^2 + m_Z^2) + (m_H^2 - m_Z^2)^2 + s^2 \right)^{3/2}} \left| \sum_f g_f^V m_f^2 N_c^f (c_f^L + c_f^R) \cdot \right. \\ &\cdot \left\{ m_H^2 \left[(-m_H^2 + m_Z^2 + s) C_0(m_H^2, m_Z^2, s, m_f^2, m_f^2, m_f^2) - 2B_0(m_H^2, m_f^2, m_f^2) \right] \right. \\ &\left. + (m_H^2 + m_Z^2 - s) B_0(m_Z^2, m_f^2, m_f^2) + (m_H^2 - m_Z^2 + s) B_0(s, m_f^2, m_f^2) \right\} \Bigg|^2. \quad (\text{A.13}) \end{aligned}$$

$$\begin{aligned} \sigma(\chi\chi \rightarrow \gamma\gamma) &= \frac{16\alpha_{\text{em}}^2 g_\chi^2 g_{Z'}^4}{\pi^3 (\Gamma_{Z'}^2 m_{Z'}^2 + (m_{Z'}^2 - s)^2)} \frac{m_\chi^2 \sqrt{s} (s - m_{Z'}^2)^2}{m_{Z'}^4 \sqrt{s - 4m_\chi^2}} \cdot \\ &\cdot \left| \sum_f g_f^A N_c^f Q_f^2 \left[2m_f^2 C_0(0, 0, s, m_f^2, m_f^2, m_f^2) + 1 \right] \right|^2, \quad (\text{A.14}) \end{aligned}$$

$$\begin{aligned} \sigma(\chi\chi \rightarrow \gamma h) &= \frac{\alpha_{\text{em}} g_\chi^2 g_{Z'}^4}{6\pi^4 (\Gamma_{Z'}^2 m_{Z'}^2 + m_{Z'}^4 - 2m_{Z'}^2 s + s^2)} \frac{\sqrt{s - 4m_\chi^2}}{s^{3/2} v^2 (s - m_H^2)} \cdot \\ &\cdot \left| \sum_f g_f^V m_f^2 N_c^f Q_f \left\{ -2s B_0(m_H^2, m_f^2, m_f^2) + 2s B_0(s, m_f^2, m_f^2) \right. \right. \\ &\left. \left. + (s - m_H^2) \left[(4m_f^2 - m_H^2 + s) C_0(m_H^2, 0, s, m_f^2, m_f^2, m_f^2) + 2 \right] \right\} \right|^2, \quad (\text{A.15}) \end{aligned}$$

$$\begin{aligned}
\sigma(\chi\chi \rightarrow \gamma Z^{(T)}) &= \frac{\alpha_{\text{em}}\alpha_W g_\chi^2 g_{Z'}^4}{3\pi^3 [(s - m_{Z'}^2)^2 + \Gamma_{Z'}^2 m_{Z'}^2] m_{Z'}^4 s^{5/2} (s - m_Z^2) \sqrt{s - 4m_\chi^2}}. \\
&\cdot \left\{ \frac{m_{Z'}^4}{2} (s - 4m_\chi^2) \left| \sum_f N_c^f Q_f \left\{ m_Z^2 s (g_f^A (c_f^L + c_f^R) + g_f^V (c_f^R - c_f^L)) (B_0(m_Z^2, m_f^2, m_f^2) - B_0(s, m_f^2, m_f^2)) \right. \right. \right. \\
&\quad - (s - m_Z^2) \left[2m_f^2 C_0(m_Z^2, 0, s, m_f^2, m_f^2, m_f^2) (g_f^A c_f^L m_Z^2 + g_f^A c_f^R m_Z^2 - c_f^L g_f^V s + c_f^R g_f^V s) \right. \\
&\quad \left. \left. \left. + m_Z^2 (g_f^A (c_f^L + c_f^R) + g_f^V (c_f^R - c_f^L)) \right] \right\} \right|^2 + 3m_\chi^2 (s - m_Z^2)^4 (s - m_{Z'}^2)^2. \\
&\cdot \left| \sum_f N_c^f Q_f \left\{ 2g_f^A m_f^2 (c_f^L + c_f^R) C_0(m_Z^2, 0, s, m_f^2, m_f^2, m_f^2) + g_f^A (c_f^L + c_f^R) + g_f^V (c_f^R - c_f^L) \right\} \right|^2, \quad \left. \right\} \quad (\text{A.16})
\end{aligned}$$

$$\begin{aligned}
\sigma(\chi\chi \rightarrow \gamma Z^{(L)}) &= \frac{\alpha_{\text{em}}\alpha_W g_\chi^2 g_{Z'}^4}{6\pi^3 [(s - m_{Z'}^2)^2 + \Gamma_{Z'}^2 m_{Z'}^2] m_{Z'}^2 s^{3/2} (s - m_Z^2)} \sqrt{s - 4m_\chi^2}. \\
&\cdot \left| \sum_f N_c^f Q_f \left\{ m_Z^2 s (g_f^A (c_f^L + c_f^R) + g_f^V (c_f^R - c_f^L)) (B_0(m_Z^2, m_f^2, m_f^2) - B_0(s, m_f^2, m_f^2)) \right. \right. \\
&\quad - (s - m_Z^2) \left[2m_f^2 C_0(m_Z^2, 0, s, m_f^2, m_f^2, m_f^2) (g_f^A c_f^L m_Z^2 + g_f^A c_f^R m_Z^2 - c_f^L g_f^V s + c_f^R g_f^V s) \right. \\
&\quad \left. \left. \left. + m_Z^2 (g_f^A (c_f^L + c_f^R) + g_f^V (c_f^R - c_f^L)) \right] \right\} \right|^2, \quad (\text{A.17})
\end{aligned}$$

$$\begin{aligned}
\sigma(\chi\chi \rightarrow hh) &= \frac{g_\chi^4 g_{Z'}^8 m_\chi^2 \cos^4 \theta}{2048\pi^5} \frac{\sqrt{s - 4m_h^2}}{s(s - 4m_\chi^2)^{3/2}}. \\
&\cdot \left| B_0(m_\chi^2, m_\chi^2, m_{Z'}^2) - B_0(s, m_{Z'}^2, m_{Z'}^2) + (2m_\chi^2 + m_{Z'}^2 - s) C_0(m_\chi^2, m_\chi^2, s, m_{Z'}^2, m_\chi^2, m_{Z'}^2) \right|^2. \quad (\text{A.18})
\end{aligned}$$

In the cross sections involving a fermionic loop, we denoted by \sum_f a sum over all the SM fermion species. In the WW cross section, instead, we denoted by \sum_i a sum over the six fermion families (three families of quarks and three of leptons), with m_{u^i}, m_{d^i} the upper and lower component of the doublet, respectively, and with $g_{u^i}^L, g_{u^i}^R, g_{d^i}^L, g_{d^i}^R$ the combinations

$$g_{u^i}^L = g_{u^i}^V - g_{u^i}^A, \quad g_{u^i}^R = g_{u^i}^V + g_{u^i}^A, \quad g_{d^i}^L = g_{d^i}^V - g_{d^i}^A, \quad g_{d^i}^R = g_{d^i}^V + g_{d^i}^A. \quad (\text{A.19})$$

The functions A_0, B_0 and C_0 are the standard Passarino-Veltman one loop one-, two- and three-points scalar integrals [70]:

$$A_0(m_0^2) = \frac{\mu^{4-D}}{i\pi^{D/2}\gamma_\Gamma} \int \frac{d^D k}{k^2 - m_0^2}, \quad (\text{A.20})$$

$$B_0(p^2, m_1^2, m_2^2) = \frac{\mu^{4-D}}{i\pi^{D/2}\gamma_\Gamma} \int \frac{d^D k}{(k^2 - m_1^2)((k+p)^2 - m_2^2)}, \quad (\text{A.21})$$

$$C_0(p_1^2, p_2^2, (p_1 + p_2)^2, m_1^2, m_2^2, m_3^2) = \frac{\mu^{4-D}}{i\pi^{D/2}\gamma_\Gamma} \int \frac{d^D k}{(k^2 - m_1^2)((k + p_1)^2 - m_2^2)((k + p_1 + p_2)^2 - m_3^2)}, \quad (\text{A.22})$$

with

$$\gamma_\Gamma = \frac{\Gamma^2(1 - \epsilon)\Gamma(1 + \epsilon)}{\Gamma(1 - 2\epsilon)}, \quad D = 4 - 2\epsilon, \quad (\text{A.23})$$

where γ_Γ approaches 1 in the limit $\epsilon \rightarrow 0$. In these equations, we denoted by $v \simeq 246$ GeV the vacuum expectation value of the Higgs field, and by c_f^L, c_f^R the SM coupling of the Z boson to left- and right-handed fermions respectively (see Tab. 3).

SM fermion f	c_f^L	c_f^R
leptons	$-\frac{1}{2} + \sin^2 \theta_W$	$\sin^2 \theta_W$
neutrinos	$\frac{1}{2}$	0
up quarks	$\frac{1}{2} - \frac{2}{3} \sin^2 \theta_W$	$-\frac{2}{3} \sin^2 \theta_W$
down quarks	$-\frac{1}{2} + \frac{1}{3} \sin^2 \theta_W$	$\frac{1}{3} \sin^2 \theta_W$

Table 3. Coupling of the Z boson to SM fermions.

Let us briefly comment on the one loop cross sections:

WW : The bosonic loop diagrams 5 and 6 in Fig. 7 are velocity suppressed as expected.

ZZ : The box diagram (number 3 on Fig. 7) is suppressed at low energies by the two heavy propagators in the loop, and gives only a minor effect. Therefore we ignored it in our calculations.

$\gamma\gamma$: The cross section for annihilation into $\gamma\gamma$ vanishes on resonance, due to the factor of $(s - m_{Z'}^2)^2$ in the numerator. This is a consequence of the Landau-Yang theorem [71, 72] that states that a spin-1 particle can not decay into two photons, and is a reassuring cross-check of our results.

Also notice that the $\gamma\gamma$ cross section is proportional to g_f^A , the axial coupling of the fermions to the Z' , and vanishes in the limit of pure $B - L$. This is due to the Dirac structure of the fermion loop in the very same way in which the cross section for annihilation into γh is proportional to the vectorial coupling g_f^V , and can be seen as a realization of the Furry theorem [73], which states that any physical amplitude involving an odd number of photons vanishes (in our case one of the photons is replaced by the vectorial part of the Z').

hh : The two diagrams with a fermionic loop (diagrams 2 and 3 in Fig. 7) sum to zero, while the two box diagrams (numbers 4 and 5) give a contribution at most comparable to that of the triangular diagram (number 1). Since the cross section for annihilation into hh including only the triangular diagram is subdominant by several orders of magnitude, we can safely ignore the contribution of the two box diagrams.

Results of our calculations show that in the low kinetic energy regime that is relevant for DM annihilation in the Sun loop channels are usually subdominant. Some of the cross

sections receive a velocity suppression ($\sigma v \simeq bv^2$) and precisely vanish in the zero velocity limit. Those are $W^{(T)}W^{(T)}$, $Z^{(T)}Z^{(L)}$, $\gamma Z^{(L)}$, γh , hh , $Z^{(T)}h$ and, for $\theta = \pi/2$, $Z^{(L)}h$. We do not explicitly show the analytical expansion around $v = 0$ because the velocity appears as an argument of the Passarino-Veltman functions. The only process, which acquires a relevant contribution at the one-loop level is $W^{(L)}W^{(L)}$.

All the cross sections we computed, except for hh that has no s -channel exchange of a Z' boson, vanish around $m_{\text{DM}} = m_{Z'}$ in the $v_{\text{DM}} \rightarrow 0$ limit. Again, this is a cross-check of the correctness of our calculations. Indeed, close to the resonance the cross section for $\chi\chi \rightarrow XX$ is proportional to the product $\Gamma(Z' \rightarrow \chi\chi) \cdot \Gamma(Z' \rightarrow XX)$, but $\Gamma(Z' \rightarrow \chi\chi)$ vanishes if $m_{\text{DM}} = m_{Z'}/2$, which is implied by a resonant production of Z' with $v_{\text{DM}} = 0$.

References

- [1] PLANCK collaboration, P. A. R. Ade et al., *Planck 2015 results. XIII. Cosmological parameters*, [1502.01589](#).
- [2] LUX collaboration, D. S. Akerib et al., *First results from the LUX dark matter experiment at the Sanford Underground Research Facility*, *Phys. Rev. Lett.* **112** (2014) 091303, [[1310.8214](#)].
- [3] B. Patt and F. Wilczek, *Higgs-field portal into hidden sectors*, [hep-ph/0605188](#).
- [4] Y. G. Kim and K. Y. Lee, *The Minimal model of fermionic dark matter*, *Phys. Rev.* **D75** (2007) 115012, [[hep-ph/0611069](#)].
- [5] PICO collaboration, C. Amole et al., *Dark Matter Search Results from the PICO-60 CF₃I Bubble Chamber*, Submitted to: *Phys. Rev. D* (2015) , [[1510.07754](#)].
- [6] LUX collaboration, D. S. Akerib et al., *First spin-dependent WIMP-nucleon cross section limits from the LUX experiment*, [1602.03489](#).
- [7] A. Gould, *Cosmological density of WIMPs from solar and terrestrial annihilations*, *Astrophys. J.* **388** (1992) 338–344.
- [8] ICECUBE collaboration, M. G. Aartsen et al., *Search for dark matter annihilations in the Sun with the 79-string IceCube detector*, *Phys. Rev. Lett.* **110** (2013) 131302, [[1212.4097](#)].
- [9] ICECUBE collaboration, M. G. Aartsen et al., *Improved limits on dark matter annihilation in the Sun with the 79-string IceCube detector and implications for supersymmetry*, [1601.00653](#).
- [10] G. Busoni, A. De Simone, E. Morgante and A. Riotto, *On the Validity of the Effective Field Theory for Dark Matter Searches at the LHC*, *Phys. Lett.* **B728** (2014) 412–421, [[1307.2253](#)].
- [11] G. Busoni, A. De Simone, J. Gramling, E. Morgante and A. Riotto, *On the Validity of the Effective Field Theory for Dark Matter Searches at the LHC, Part II: Complete Analysis for the s -channel*, *JCAP* **1406** (2014) 060, [[1402.1275](#)].
- [12] G. Busoni, A. De Simone, T. Jacques, E. Morgante and A. Riotto, *On the Validity of the Effective Field Theory for Dark Matter Searches at the LHC Part III: Analysis for the t -channel*, *JCAP* **1409** (2014) 022, [[1405.3101](#)].
- [13] O. Buchmueller, M. J. Dolan and C. McCabe, *Beyond Effective Field Theory for Dark Matter Searches at the LHC*, *JHEP* **01** (2014) 025, [[1308.6799](#)].
- [14] D. Racco, A. Wulzer and F. Zwirner, *Robust collider limits on heavy-mediator Dark Matter*, *JHEP* **05** (2015) 009, [[1502.04701](#)].

- [15] J. Fan, M. Reece and L.-T. Wang, *Non-relativistic effective theory of dark matter direct detection*, *JCAP* **1011** (2010) 042, [[1008.1591](#)].
- [16] A. L. Fitzpatrick, W. Haxton, E. Katz, N. Lubbers and Y. Xu, *The Effective Field Theory of Dark Matter Direct Detection*, *JCAP* **1302** (2013) 004, [[1203.3542](#)].
- [17] A. L. Fitzpatrick, W. Haxton, E. Katz, N. Lubbers and Y. Xu, *Model Independent Direct Detection Analyses*, [1211.2818](#).
- [18] N. Anand, A. L. Fitzpatrick and W. C. Haxton, *Weakly interacting massive particle-nucleus elastic scattering response*, *Phys. Rev.* **C89** (2014) 065501, [[1308.6288](#)].
- [19] M. Cirelli, N. Fornengo and A. Strumia, *Minimal dark matter*, *Nucl. Phys.* **B753** (2006) 178–194, [[hep-ph/0512090](#)].
- [20] M. Cirelli and A. Strumia, *Minimal Dark Matter: Model and results*, *New J. Phys.* **11** (2009) 105005, [[0903.3381](#)].
- [21] Z. Bern, P. Gondolo and M. Perelstein, *Neutralino annihilation into two photons*, *Phys. Lett.* **B411** (1997) 86–96, [[hep-ph/9706538](#)].
- [22] L. Bergstrom and P. Ullio, *Full one loop calculation of neutralino annihilation into two photons*, *Nucl. Phys.* **B504** (1997) 27–44, [[hep-ph/9706232](#)].
- [23] O. Lebedev and Y. Mambrini, *Axial dark matter: The case for an invisible Z'* , *Phys. Lett.* **B734** (2014) 350–353, [[1403.4837](#)].
- [24] F. Kahlhoefer, K. Schmidt-Hoberg, T. Schwetz and S. Vogl, *Implications of unitarity and gauge invariance for simplified dark matter models*, *JHEP* **02** (2016) 016, [[1510.02110](#)].
- [25] N. F. Bell, Y. Cai and R. K. Leane, *Mono- W Dark Matter Signals at the LHC: Simplified Model Analysis*, *JCAP* **1601** (2016) 051, [[1512.00476](#)].
- [26] O. Buchmueller, M. J. Dolan, S. A. Malik and C. McCabe, *Characterising dark matter searches at colliders and direct detection experiments: Vector mediators*, *JHEP* **01** (2015) 037, [[1407.8257](#)].
- [27] M. Blennow, J. Herrero-Garcia, T. Schwetz and S. Vogl, *Halo-independent tests of dark matter direct detection signals: local DM density, LHC, and thermal freeze-out*, *JCAP* **1508** (2015) 039, [[1505.05710](#)].
- [28] A. Alves, S. Profumo and F. S. Queiroz, *The dark Z' portal: direct, indirect and collider searches*, *JHEP* **04** (2014) 063, [[1312.5281](#)].
- [29] A. Alves, A. Berlin, S. Profumo and F. S. Queiroz, *Dark Matter Complementarity and the Z' Portal*, *Phys. Rev.* **D92** (2015) 083004, [[1501.03490](#)].
- [30] A. Alves, A. Berlin, S. Profumo and F. S. Queiroz, *Dirac-fermionic dark matter in $U(1)_X$ models*, *JHEP* **10** (2015) 076, [[1506.06767](#)].
- [31] H. An, X. Ji and L.-T. Wang, *Light Dark Matter and Z' Dark Force at Colliders*, *JHEP* **07** (2012) 182, [[1202.2894](#)].
- [32] H. An, R. Huo and L.-T. Wang, *Searching for Low Mass Dark Portal at the LHC*, *Phys. Dark Univ.* **2** (2013) 50–57, [[1212.2221](#)].
- [33] M. T. Frandsen, F. Kahlhoefer, A. Preston, S. Sarkar and K. Schmidt-Hoberg, *LHC and Tevatron Bounds on the Dark Matter Direct Detection Cross-Section for Vector Mediators*, *JHEP* **07** (2012) 123, [[1204.3839](#)].

- [34] G. Arcadi, Y. Mambrini, M. H. G. Tytgat and B. Zaldivar, *Invisible Z' and dark matter: LHC vs LUX constraints*, *JHEP* **03** (2014) 134, [[1401.0221](#)].
- [35] I. M. Shoemaker and L. Vecchi, *Unitarity and Monojet Bounds on Models for DAMA, CoGeNT, and CRESST-II*, *Phys. Rev.* **D86** (2012) 015023, [[1112.5457](#)].
- [36] M. T. Frandsen, F. Kahlhoefer, S. Sarkar and K. Schmidt-Hoberg, *Direct detection of dark matter in models with a light Z'* , *JHEP* **09** (2011) 128, [[1107.2118](#)].
- [37] P. Gondolo, P. Ko and Y. Omura, *Light dark matter in leptophobic Z' models*, *Phys. Rev.* **D85** (2012) 035022, [[1106.0885](#)].
- [38] M. Fairbairn and J. Heal, *Complementarity of dark matter searches at resonance*, *Phys. Rev.* **D90** (2014) 115019, [[1406.3288](#)].
- [39] P. Harris, V. V. Khoze, M. Spannowsky and C. Williams, *Constraining Dark Sectors at Colliders: Beyond the Effective Theory Approach*, *Phys. Rev.* **D91** (2015) 055009, [[1411.0535](#)].
- [40] M. Chala, F. Kahlhoefer, M. McCullough, G. Nardini and K. Schmidt-Hoberg, *Constraining Dark Sectors with Monojets and Dijets*, *JHEP* **07** (2015) 089, [[1503.05916](#)].
- [41] T. Jacques and K. Nordström, *Mapping monojet constraints onto Simplified Dark Matter Models*, *JHEP* **06** (2015) 142, [[1502.05721](#)].
- [42] A. J. Brennan, M. F. McDonald, J. Gramling and T. D. Jacques, *Collide and Conquer: Constraints on Simplified Dark Matter Models using Mono-X Collider Searches*, [1603.01366](#).
- [43] P. Agrawal, Z. Chacko, C. Kilic and R. K. Mishra, *A Classification of Dark Matter Candidates with Primarily Spin-Dependent Interactions with Matter*, [1003.1912](#).
- [44] J. Abdallah et al., *Simplified Models for Dark Matter and Missing Energy Searches at the LHC*, [1409.2893](#).
- [45] S. Weinberg, *The quantum theory of fields. Vol. 2: Modern applications*. Cambridge University Press, 2013.
- [46] R. W. Robinett and J. L. Rosner, *Mass Scales in Grand Unified Theories*, *Phys. Rev.* **D26** (1982) 2396.
- [47] CMS collaboration, V. Khachatryan et al., *Search for physics beyond the standard model in dilepton mass spectra in proton-proton collisions at $\sqrt{s} = 8$ TeV*, *JHEP* **04** (2015) 025, [[1412.6302](#)].
- [48] CMS collaboration, S. Chatrchyan et al., *Measurement of inclusive W and Z boson production cross sections in pp collisions at $\sqrt{s} = 8$ TeV*, *Phys. Rev. Lett.* **112** (2014) 191802, [[1402.0923](#)].
- [49] J. Alwall, R. Frederix, S. Frixione, V. Hirschi, F. Maltoni, O. Mattelaer et al., *The automated computation of tree-level and next-to-leading order differential cross sections, and their matching to parton shower simulations*, *JHEP* **07** (2014) 079, [[1405.0301](#)].
- [50] CMS COLLABORATION collaboration, *Search for a Narrow Resonance Produced in 13 TeV pp Collisions Decaying to Electron Pair or Muon Pair Final States*, Tech. Rep. CMS-PAS-EXO-15-005, CERN, Geneva, 2015.
- [51] P. Gondolo and G. Gelmini, *Cosmic abundances of stable particles: Improved analysis*, *Nucl. Phys.* **B360** (1991) 145–179.

- [52] K. Griest and D. Seckel, *Three exceptions in the calculation of relic abundances*, *Phys. Rev.* **D43** (1991) 3191–3203.
- [53] M. Cirelli, E. Del Nobile and P. Panci, *Tools for model-independent bounds in direct dark matter searches*, *JCAP* **1310** (2013) 019, [[1307.5955](#)].
- [54] CMS collaboration, V. Khachatryan et al., *Search for dark matter, extra dimensions, and unparticles in monojet events in proton–proton collisions at $\sqrt{s} = 8$ TeV*, *Eur. Phys. J.* **C75** (2015) 235, [[1408.3583](#)].
- [55] ICECUBE collaboration, A. Achterberg et al., *First Year Performance of The IceCube Neutrino Telescope*, *Astropart. Phys.* **26** (2006) 155–173, [[astro-ph/0604450](#)].
- [56] ICECUBE collaboration, T. Montaruli, *Neutrino Physics and Astrophysics with IceCube*, in *Cosmic Ray International Seminar: The status and the future of the UHE Cosmic Ray Physics in the post LHC era (CRIS 2015) Gallipoli, Italy, September 14-16, 2015*, 2015. [1512.07978](#).
- [57] G. Jungman, M. Kamionkowski and K. Griest, *Supersymmetric dark matter*, *Phys. Rept.* **267** (1996) 195–373, [[hep-ph/9506380](#)].
- [58] P. Ciafaloni, D. Comelli, A. Riotto, F. Sala, A. Strumia and A. Urbano, *Weak Corrections are Relevant for Dark Matter Indirect Detection*, *JCAP* **1103** (2011) 019, [[1009.0224](#)].
- [59] M. Cirelli, G. Corcella, A. Hektor, G. Hutsi, M. Kadastik, P. Panci et al., *PPPC 4 DM ID: A Poor Particle Physicist Cookbook for Dark Matter Indirect Detection*, *JCAP* **1103** (2011) 051, [[1012.4515](#)].
- [60] P. Baratella, M. Cirelli, A. Hektor, J. Pata, M. Piibeleht and A. Strumia, *PPPC 4 DMv: a Poor Particle Physicist Cookbook for Neutrinos from Dark Matter annihilations in the Sun*, *JCAP* **1403** (2014) 053, [[1312.6408](#)].
- [61] J. Braun, J. Dumm, F. De Palma, C. Finley, A. Karle and T. Montaruli, *Methods for point source analysis in high energy neutrino telescopes*, *Astropart. Phys.* **29** (2008) 299–305, [[0801.1604](#)].
- [62] ICECUBE collaboration, M. Rameez et al., “Search for dark matter annihilations in the Sun using the completed IceCube neutrino telescope.” http://pos.sissa.it/archive/conferences/236/1209/ICRC2015_1209.pdf, 2015.
- [63] G. Punzi, *Comments on likelihood fits with variable resolution*, *eConf* **C030908** (2004) WELT002 235, [[physics/0401045](#)].
- [64] M. Drees and M. M. Nojiri, *The Neutralino relic density in minimal $N = 1$ supergravity*, *Phys. Rev.* **D47** (1993) 376–408, [[hep-ph/9207234](#)].
- [65] K. Hagiwara, R. D. Peccei, D. Zeppenfeld and K. Hikasa, *Probing the Weak Boson Sector in $e^+ e^- \rightarrow W^+ W^-$* , *Nucl. Phys.* **B282** (1987) 253–307.
- [66] G. J. Gounaris, J. Layssac and F. M. Renard, *New and standard physics contributions to anomalous Z and gamma selfcouplings*, *Phys. Rev.* **D62** (2000) 073013, [[hep-ph/0003143](#)].
- [67] R. Catena and B. Schwabe, *Form factors for dark matter capture by the Sun in effective theories*, *JCAP* **1504** (2015) 042, [[1501.03729](#)].
- [68] J. Blumenthal, P. Gretsikov, M. Krämer and C. Wiebusch, *Effective field theory interpretation of searches for dark matter annihilation in the Sun with the IceCube Neutrino Observatory*, *Phys. Rev.* **D91** (2015) 035002, [[1411.5917](#)].

- [69] J. Heisig, M. Krämer, M. Pellen and C. Wiebusch, *Constraints on Majorana Dark Matter from the LHC and IceCube*, *Phys. Rev.* **D93** (2016) 055029, [[1509.07867](#)].
- [70] G. Passarino and M. J. G. Veltman, *One Loop Corrections for $e^+ e^-$ Annihilation Into $\mu^+ \mu^-$ in the Weinberg Model*, *Nucl. Phys.* **B160** (1979) 151.
- [71] L. D. Landau, *On the angular momentum of a system of two photons*, *Dokl. Akad. Nauk Ser. Fiz.* **60** (1948) 207–209.
- [72] C.-N. Yang, *Selection Rules for the Dematerialization of a Particle Into Two Photons*, *Phys. Rev.* **77** (1950) 242–245.
- [73] S. Weinberg, *The Quantum theory of fields. Vol. 1: Foundations*. Cambridge University Press, 2005.